THE JOURNAL OF BIOLOGICAL CHEMISTRY VOL. 288, NO. 38, pp. 27181–27199, September 20, 2013

A Stable Bacterial Peroxidase with Novel Halogenating Activity and an Autocatalytically Linked Heme Prosthetic Group*

Received for publication, April 25, 2013, and in revised form, August 2, 2013 Published, JBC Papers in Press, August 5, 2013, DOI 10.1074/jbc.M113.477067

Markus Auer[‡], Clemens Gruber[‡], Marzia Bellei[§], Katharina F. Pirker[‡], Marcel Zamocky[‡¶], Daniela Kroiss[‡], Stefan A. Teufer[‡], Stefan Hofbauer[‡], Monika Soudi[‡], Gianantonio Battistuzzi[‖], Paul G. Furtmüller[‡], and Christian Obinger[‡1]

From the [‡]Division of Biochemistry, Department of Chemistry, Vienna Institute of BioTechnology, BOKU-University of Natural Resources and Life Sciences, Muthgasse 18, A-1190 Vienna, Austria, the Departments of [§]Life Sciences and [‖]Chemistry and Geology, University of Modena and Reggio Emilia, 41100 Modena, Italy, and the [¶]Institute of Molecular Biology, Slovak Academy of Sciences, 84551 Bratislava, Slovakia

Background: First analysis was made of bacterial ancestor of peroxidases from mammalian innate immune system.
Results: Highly stable heme enzyme possesses high bromination activity and covalently bound prosthetic group.
Conclusion: Post-translational autocatalytic (peroxide-driven) heme modification is found in prokaryotic and eukaryotic halogenating peroxidases.
Significance: Peroxidase-mediated production of antimicrobial hypohalous acids was developed early in evolution.

Reconstructing the phylogenetic relationships of the main evolutionary lines of the mammalian peroxidases lactoperoxidase and myeloperoxidase revealed the presence of novel bacterial heme peroxidase subfamilies. Here, for the first time, an ancestral bacterial heme peroxidase is shown to possess a very high bromide oxidation activity (besides conventional peroxidase activity). The recombinant protein allowed monitoring of the autocatalytic peroxide-driven formation of covalent heme to protein bonds. Thereby, the high spin ferric rhombic heme spectrum became similar to lactoperoxidase, the standard reduction potential of the Fe(III)/Fe(II) couple shifted to more positive values (−145 ± 10 mV at pH 7), and the conformational and thermal stability of the protein increased significantly. We discuss structure-function relationships of this new peroxidase in relation to its mammalian counterparts and ask for its putative physiological role.

Today, heme peroxidases are assigned to two distinct superfamilies (the peroxidase-catalase superfamily (1) and the peroxidase-cyclooxygenase superfamily (2)) and to three smaller families (3) (heme-thiolate peroxidases or heme aromatic peroxygenases, DyP-type peroxidases, and di-heme cytochrome *c* peroxidases). This work focuses on a new subfamily within the peroxidase-cyclooxygenase superfamily (2).

Reconstruction of the phylogeny of the peroxidase-cyclooxygenase superfamily revealed the occurrence of seven subfamilies (2). Subfamily 1 is already well investigated and composed of vertebrate peroxidases, including myeloperoxidase (MPO),[2] eosinophil peroxidase (EPO), lactoperoxidase (LPO), and thyroid peroxidase (TPO). The main catalytic activity of these oxidoreductases is the two-electron oxidation of halides or thiocyanate mediated by hydrogen peroxide. The released antimicrobial hypohalous acids and hypothiocyanite (4, 5) play a role in the innate immune system (MPO, EPO, and LPO) or in hormone biosynthesis (TPO) (6). Some biochemical data are found in the literature about subfamilies 2 and 3 (peroxidasins (7) and peroxinectins (8)) of the peroxidase-cyclooxygenase superfamily. Enzymes from both clades are multidomain proteins with the peroxidase domain being associated with other (nonenzymatic) domains that mediate protein-protein interaction(s). They are also reported to catalyze the oxidation of halides and to participate in innate immunity as well as in tissue biogenesis (7, 8).

By contrast, nothing is known about two other heme peroxidase subfamilies, which have been named peroxicins (subfamily 5) and peroxidockerins (subfamily 6) (2). Fig. 1 depicts the unrooted phylogenetic tree of 140 sequences used for the analysis with focus on these two clades. Peroxicins were formed early in evolution, and a high proportion of members is encoded by extremely long (pseudo)genes, where the peroxidase domain or at least some motifs can be repeated several times. Moreover, these large fusion proteins contain hemolysin-type toxin and Ca^{2+}-binding motifs (2) that could indicate a role in the defense of bacteria against other organisms (2, 9). Metalloproteins from the sixth subfamily (peroxidockerins) are also multidomain proteins with one membrane anchor and sequence motifs (*e.g.* dockerin-like domains) characteristic for

* This work was supported by Austrian Science Funds FWF Projects P20664 and P25538 and Doctoral Program BioToP-Biomolecular Technology of Proteins FWF Project W1224.
[1] To whom correspondence should be addressed. Tel.: 43-1-47654-6073; Fax: 43-1-47654-6059; E-mail: christian.obinger@boku.ac.at.
[2] The abbreviations used are: MPO, myeloperoxidase; LspPOX, recombinant heme peroxidase from *Lyngbya* sp., PCC 8106 as produced by *E. coli*; LspPOX (H_2O_2), recombinant heme peroxidase from *Lyngbya* sp. PCC 8106 preincubated with the 15× stoichiometric excess of hydrogen peroxide for 1 h at room temperature; LPO, bovine lactoperoxidase; EPO, eosinophil peroxidase; ABTS, 2,2′-azinodi-(3-ethylbenzthiazoline-6-sulfonic acid); TauBr, taurine monobromamine; TauCl, taurine monochloramine; MCD, monochlorodimedone; ECD, electronic circular dichroism; DSC, differential scanning calorimetry.

extracellular proteins (2). Besides bacteria, a few primitive eukaryotes (*e.g. Dictyostelium* species) also contain genes encoding these peroxidases (Fig. 1).

To gain more insight into the catalytic activity of these so far unexplored oxidoreductases, we have analyzed the peroxidase domains of representatives of both clades and saw a high homology with the well studied mammalian peroxidases. Sequence alignment (Fig. 2) suggested a similar proximal and distal architecture. These *in silico* data (Figs. 1 and 2) prompted us to choose one representative for a comprehensive biochemical and biophysical investigation. In detail, we selected a cyanobacterial enzyme from *Lyngbya* sp. PCC 8106 as there seems to be a direct lineage from this bacterial oxidoreductase to the mammalian peroxidases (Fig. 1). This first investigated member of the peroxidockerin clade could easily be produced in *Escherichia coli* with almost 100% heme occupancy. It exhibited a high bromination, low chlorination, and broad peroxidase activity at high conformational and thermal stability. The recombinant enzyme for the first time allowed monitoring of the autocatalytic formation of covalent heme to protein bonds by a broad set of techniques, including UV-visible, ECD, and EPR spectroscopy, mass spectrometry, spectroelectrochemistry, and differential scanning calorimetry. These findings are discussed with respect to published structure-function relationships of LPO, EPO, and MPO, the putative physiological role of these metalloenzymes in bacteria, and their potential application in biotechnology.

EXPERIMENTAL PROCEDURES

Chemicals and enzymes were from the following sources: ABTS, guaiacol, PMSF, hemin, hydrogen peroxide, and bovine lactoperoxidase were from Sigma; acetonitrile (HiPerSolv Chromanorm) MS-grade was from Prolabo; formic acid was from Acros Organics; sequencing grade modified trypsin was from Promega; GluC (sequencing grade) was from Roche Applied Science; QIAEX II extraction kit was from Qiagen; pET-21a (+) vector was from Invitrogen; T7 expression system was from Novagen; chelating Sepharose Fast Flow column was from Amersham Biosciences; hydroxyapatite column was from Sigma; and Centriprep-50 concentrators were from Amicon. Highly purified human myeloperoxidase was purchased from Planta Natural Products. All other chemicals were of the highest purity grade available. Hydrogen peroxide was obtained as a 30% solution, and after dilution, the concentration was measured using the extinction coefficient of 39.4 M^{-1} cm^{-1} at 240 nm.

Phylogenetic Analysis—The evolutionary history of 140 full-length protein sequences was inferred using the maximum likelihood method of the MEGA 5.05 package (10) with 100 bootstrap replications used as a statistical support. The evolutionary distances were computed using the Whelan and Goldman method (11) and are presented as the number of amino acid substitutions per site. There were a total of 5238 analyzed positions in the final dataset. The reconstructed phylogenetic tree was presented with the Tree Explorer of this package. Abbreviations of sequence names correspond with PeroxiBase (12).

Structural Alignment of Peroxidase Sequences—Multiple sequence alignment of 20 selected protein sequences from the dataset used for phylogenetic reconstruction was performed using the Muscle program implemented in the MEGA 5.05 package (10) with the UPGMB clustering method and up to 1000 iterations. This alignment included also a sequence of bovine lactoperoxidase with known three-dimensional structure (13). The pre-aligned sequences served as input for structural alignment conducted with the ESPript method (14), and Protein Data Bank code 3BXI, chain A (lactoperoxidase), served as the reference three-dimensional structure. The ESPript program calculated a similarity score for each involved residue of aligned sequences, and in the output the secondary structure elements were numbered and located in corresponding positions above the multiple sequence alignment.

Cloning, Expression, and Purification of Lyngbya sp. PCC 8106 Peroxidase (LspPOX)—The cyanobacterial strain *Lyngbya* sp. (PCC 8106) was ordered from the Pasteur culture collection (PCC) in Paris, France. The peroxidase gene was amplified from genomic DNA and inserted into the pET-21a(+) vector (Invitrogen). The *E. coli* host strain (Invitrogen) BL21Star (DE3) carrying the pET-21a(+) plasmid containing the wild-type peroxidase gene of *Lyngbya* sp. PCC 8106 (*E. coli* BL21Star(DE3)/pET-21a(+)/LspPOX) was used for expression with the T7 expression system (Novagen). Plasmid preparation, PCR, and restriction screening were carried out in *E. coli* TOP10 cells. The plasmid was isolated from the cells and transferred into *E. coli* BL21Star (DE3) strain by chemical transformation for final expression screening and protein preparation.

Overnight cultures of *E. coli* BL21Star (DE3) containing the LspPOX gene were grown in 12 ml of LBamp medium at 37 °C on a shaker (180 rpm) and used as inoculum for 1 liter of M9ZB-amp medium. The cultures were grown in two 2-liter Erlenmeyer flasks at 37 °C and 180 rpm until the absorbance at 600 nm (A_{600}) reached a value of 0.9–1.2. Expression of *Lyngbya* sp. peroxidase was induced with 100 ml of 5% (w/v) lactose solution (5 g/liter final concentration) supplemented with 50 mg/liter hemin. The cells were grown overnight at 16 °C with shaking at 180 rpm. To harvest the cells, the cultures were centrifuged at 2700 × *g* and 4 °C for 5 min. The pellet was resuspended and transferred to Falcon tubes. Cells were centrifuged at 950 × *g*, 4 °C for 20 min, and the pellet was stored at −80 °C.

A hexa-histidine tag (His_6 tag) has been C-terminally fused to the LspPOX gene. Consequently, the peroxidase was purified with metal chelate affinity chromatography. The cell pellet of 1 liter of *E. coli* culture was thawed and resuspended in 40 ml of lysis buffer (50 mM Tris-HCl, pH 8.0, containing 2 mM Na_2EDTA, 0.1% Triton X-100, 1 mM PMSF). The cell suspension was cooled on ice during lysis by ultrasonic treatment (50% pulse, four times for 30 s) and then centrifuged at 27,000 × *g* at 4 °C for 20 min. The pellet was discarded, and the supernatant containing the soluble LspPOX was used for metal chelate affinity chromatography. After addition of 1 M NaCl and 20 mM imidazole (final concentration), the solution was loaded on a chelating Sepharose gel column (1.6 cm × 10 cm) charged with Ni^{2+} (5 mg/ml) and equilibrated with 100 mM phosphate buffer, pH 7.0, containing 1 M NaCl and 20 mM imidazole at 4 °C. The column was washed with equilibration buffer, and bound proteins were eluted with 100 ml of a gradient of 20–500 mM imidazole in equilibration buffer. The collected protein was

desalted with PD-10 columns and eluted in 5 mM phosphate buffer, pH 7.4, and then applied to a hydroxylapatite (HA) column equilibrated with 5 mM sodium phosphate, pH 7.4. After washing the HA column with 5 mM phosphate buffer, the elution was performed stepwise with increasing phosphate concentrations (20, 50, 100, and 200 mM; pH 7.4). Fractions at 50 and 100 mM sodium phosphate, which showed the Soret maximum at 412 nm, were collected. The protein was concentrated by ultrafiltration (Amicon CentriPrep) with an exclusion size of 50 kDa, desalted with PD-10 columns, and stored in 10 mM phosphate buffer, pH 7.0, at −80 °C.

UV-Visible Spectroscopy—UV-visible spectra of recombinant LspPOX and LspPOX pretreated with the 15 times molar excess of hydrogen peroxide at room temperature, *i.e.* LspPOX (H_2O_2), were recorded with an Hitachi U-3900 spectrophotometer in the range of 200–800 nm at 25 °C. The molar extinction coefficient of the ferric high spin LspPOX at a Soret maximum of $\epsilon_{412\,nm}$ = 94,670 M^{-1} cm^{-1} was obtained from the plot of absorbance at 412 mm *versus* protein concentration determined by the method of Bradford (15). It was used for calculation of LspPOX concentrations throughout this work.

Stopped-flow Spectroscopy—Transient state kinetics was performed to study the reduction pathway of ferric LspPOX and LspPOX (H_2O_2) by freshly prepared dithionite in solution in comparison with LPO and HRP. The experiments were carried out with a stopped-flow apparatus (model SX-18MV, Applied Photophysics) equipped in the conventional mode. The optical quartz cell with a pathlength of 10 mm had a volume of 20 μl. The fastest time for mixing two solutions and recording the first data point was 1.3 ms. All measurements were performed at 25 °C. A minimum of three measurements was performed for each protein. The reactions were followed with the diode array detector (Applied Photophysics), which allowed the synthesis of artificial sets of time-dependent spectra as well as analysis of time traces.

Conventional stopped-flow spectroscopy was performed to directly monitor the formation of taurine chloramine at 253 nm (ϵ_{253} = 429 M^{-1} cm^{-1}) and taurine bromamine at 289 nm (ϵ_{289} = 415 M^{-1} cm^{-1}). 100 nM enzyme, 10 mM taurine, 200 μM H_2O_2 were mixed with either 100 mM NaCl or KBr from pH 4.0 to pH 9.0. Buffer contained the following: 100 mM carbonate buffer, pH 8.0–9.0, 100 mM phosphate buffer, pH 5.0–8.0, or 100 mM citrate/phosphate buffer, pH 4.0–5.0. Rates of TauBr and TauCl formation were obtained by fitting the initial (linear) phase of the obtained time traces. One unit of halogenation activity was defined as the amount of enzyme that halogenates 1 μmol of taurine per min at 25 °C.

Spectroelectrochemistry—Determination of the standard reduction potential, $E^{0\prime}$, of the Fe(III)/Fe(II) couple was carried out using a homemade OTTLE (optically transparent thin layer spectroelectrochemical) cell (16–18). The three-electrode configuration consisted of a gold mini-grid working electrode (Buckbee-Mears), a homemade Ag/AgCl/KCl_{sat} micro-reference electrode, separated from the working solution by a Vycor set, and a platinum wire as counter-electrode (16–18). The reference electrode was calibrated against a saturated calomel (Hg_2Cl_2) electrode before each set of measurements. All potentials are referenced to the standard hydrogen electrode. Potentials were applied across the OTTLE cell with an Amel model 2053 potentiostat/galvanostat. A constant temperature was maintained by a circulating water bath, and the OTTLE cell temperature was monitored with a copper-costan microthermocouple. UV-visible spectra were recorded using a Varian Cary C50 spectrophotometer. Spectroelectrochemical titrations were carried out using samples containing 10 μM LspPOX or 12 μM LspPOX (H_2O_2) dissolved in 100 mM phosphate buffer and 100 mM NaCl at pH 7.0, in the presence of 80 μM (LspPOX) or 100 μM (LspPOX (H_2O_2)) methyl viologen and 2 μM lumiflavin 3-acetate, methylene blue, phenazine methosulfate, and indigo disulfonate used as mediators.

EPR Spectroscopy—For EPR measurements, 100 μM recombinant LspPOX and LspPOX (H_2O_2) as well as LPO as reference protein were prepared in 100 mM phosphate buffer, pH 7.0. Solutions of 100 μl were transferred in Wilmad quartz tubes (inner diameter 3 mm) and frozen in liquid nitrogen. The tube was then flushed with argon and kept frozen on dry ice.

LspPOX (H_2O_2) was prepared by the addition of a 15× molar excess of H_2O_2 to 100 μM LspPOX. The solution was kept at room temperature for 1 h before being frozen in liquid nitrogen.

Measurements were carried out at 10 K on a Bruker ESP300 continuous wave spectrometer, operating at X-band (9 GHz) frequencies, equipped with a TE resonator and a helium cryostat from Oxford Instruments (ESR900). EPR spectra were recorded under nonsaturating conditions for high spin systems, using 20-milliwatt microwave power, 100 kHz modulation frequency, 1 millitesla modulation amplitude, and 20 ms conversion time and time constant. Simulations of EPR spectra include a weighted sum of individual high spin Fe(III) forms using the software EasySpin (41). Based on these simulations, the rhombicity and effective *g* values for each high spin compound were determined.

Mass Spectrometry—For determination of the overall molar mass, 5 μg of LspPOX or LspPOX (H_2O_2) were directly injected to the LC-MS system (Dionex Ultimate 3000 LC, MS: Bruker, maXis 4G ETD, equipped with the standard ESI source). The protein solution was eluted by developing a linear gradient from 15 to 70% acetonitrile (Supelco Discovery Bio Wide Pore C5 column, 50 × 0.32 mm, 3 μm packing). Data were processed using Data Analysis 4.0 (Bruker), and the spectra were deconvoluted by Max Ent.

For peptide mass mapping, 10 μg of LspPOX or LspPOX (H_2O_2) were digested by GluC/trypsin (enzyme/substrate ratio 1:50 in 100 mM ammonium bicarbonate buffer) overnight at 37 °C followed by LC-MS analysis in positive mode. The HPLC (Dionex Ultimate 3000) was equipped with a C18 column (Thermo BioBasic, 150 × 0.32 mm, 5-μm particle size). Elution of peptides was achieved by a linear gradient from 4 to 80% B within 50 min (A, 65 mM ammonium formate buffer; B, 100% acetonitrile). Mass spectrometer Bruker maXis 4G ETD equipped with standard ESI source was used.

For detection of modification(s) at the prosthetic group, 30 μg of LspPOX (H_2O_2) were digested with GluC/trypsin (enzyme/substrate ratio 1:20 in 100 mM ammonium bicarbonate buffer and 2 M urea) overnight at 37 °C. After addition of 3 M hydrochloric acid at 70 °C for 10 min, the sample was centri-

fuged, and the pellet was solved by stepwise addition of 3 M ammonia to a final pH of 7.0. Finally, LC-MS analysis was performed as described above.

For determination of the formation of TauBr by LspPOX, 500 nM enzyme were incubated with 5 mM taurine, 500 μM H_2O_2, 50 mM KBr in 5 mM citric buffer, pH 7.0, at room temperature for 10 min. Measurements were performed by direct infusion (50 μl) in negative mode. The same conditions were used for determination of TauCl, except for usage of 50 mM NaCl and 5 mM citric buffer, pH 5.0.

Steady-state Kinetics—Besides following the formation of TauCl and TauBr by stopped-flow spectroscopy, halogenation activity was also probed spectrophotometrically (Hitachi U-3900, Zeiss Specord 10) using the monochlorodimedone (MCD) assay (19). In detail, MCD (100 μM) was dissolved either in 100 mM carbonate buffer, pH 8.0–10.0, 100 mM phosphate buffer, pH 5.0–8.0, or 100 mM citrate/phosphate buffer, pH 4.0–5.0, containing either bromide or chloride (each 100 mM) and 50 nM LspPOX or bovine LPO or human MPO as a reference enzyme (22, 23). Upon addition of 100 μM H_2O_2, MCD was converted into the dihalogenated product. However, MCD was also oxidized by LspPOX in the absence of halides suggesting that the observed decrease in absorbance was due to both the halogenation activity and the oxidation of MCD by the LspPOX/H_2O_2 system. Interestingly, this effect was much more pronounced with LspPOX compared with MPO (19). Depending on pH, 31–50% of the decrease in absorbance could be attributed to the MCD oxidation by LspPOX. Thus, rates of halogenation were determined from the initial linear part of the adjusted time traces (*i.e.* subtraction of contribution of MCD oxidation reaction) using an extinction coefficient for MCD at 290 nm of 19.9 mM^{-1} cm^{-1} (19). One unit of halogenation activity was defined as the amount of enzyme that halogenates 1 μmol of MCD/min at 25 °C.

Peroxidase activity was tested with the artificial one-electron donors guaiacol (100 μM) and (1 mM) ABTS in 100 mM phosphate buffer, pH 7.0. Rates of guaiacol or ABTS oxidation were calculated by following the absorbance increase at 470 nm (ϵ_{470} = 26.6 mM^{-1} cm^{-1}) (20) and 414 nm (ϵ_{414} = 36 mM^{-1} cm^{-1}) (21), respectively. For the enzyme, 50 nM (in guaiacol oxidation assays) or 2.5 nM (in ABTS oxidation assays) was used; for H_2O_2, 100 μM was used. One unit of peroxidase activity was defined as the amount that oxidizes 1 μmol of substrate/min at defined pH values and at 25 °C. The activity was measured in the pH range 4.0–9.0 (100 mM carbonate buffer, pH 8.0–10.0, 100 mM phosphate buffer, pH 5.0–8.0, or 100 mM citrate/phosphate buffer, pH 4.0–5.0).

For determination of the effect of temperature on enzyme activity, the protein was kept at the respective temperature (20–90 °C) for 5 min and then slowly brought to room temperature for kinetic analysis. For bromination assay, 100 mM bromide, 100 μM H_2O_2, 5 nM enzyme, 100 mM phosphate buffer, pH 7.0, was used; for the ABTS assay, 1 mM ABTS, 100 μM H_2O_2, 25 nM enzyme, 100 mM phosphate buffer, pH 7.0, was used.

Unfolding Studies—Temperature-mediated unfolding was followed by electronic circular dichroism (ECD) spectroscopy as well as differential scanning calorimetry (DSC). ECD was performed using Chirascan (Applied Photophysics, Leatherhead, UK), which allowed simultaneous UV-visible and ECD monitoring and was equipped with a Peltier temperature control unit for a stepwise temperature increase (2 °C) at defined incubation times. The machine was flushed with nitrogen with a flow rate of 5 liters/min. In the near-UV and visible region (250–500 nm), the instrument parameters were set as follows: path length, 10 mm; spectral bandwidth, 1 nm; step size, 1 nm, scan time per point, 0.5 s (scan period, 25 μs × 20,000 counts); and scan time, ~125 s. In addition single wavelength scans at 409 nm (Soret region) were performed with the same instrumental setup mentioned above. Temperature-mediated changes in the far-UV region were recorded by following changes in ellipticity at 208 nm. The path length was 1 mm, spectral bandwidth was 2 nm, and scan time per point was 12 s (scan period was 25 μs × 480,000 counts).

DSC measurements were performed using a VP-DSC microcalorimeter from MicroCal controlled by the VP-viewer program and equipped with a 137-μl cell. Studies were made with 4 μM of protein in 10 mM buffer in the presence of 0.5 M GdnHCl. Buffers used were as follows: 10 mM carbonate buffer (pH 9.0–11.0), phosphate buffer (pH 5.0–8.0), and citrate/phosphate buffer (pH 3.0–5.0). Samples were analyzed using a programmed heating scan rate of 90 °C/h (1.5 °C per min) and ~4.1 bar cell pressure over a temperature range of 20–100 °C. Collected DSC data were corrected for base line with buffer and normalized for protein concentration. The heat capacity (C_p) was expressed in kcal mol^{-1} K^{-1} (1 cal = 4.184 J). Data analysis was performed with MicroCal Origin software. Individual endotherms were fitted by a two-state model using the Lavenberg/Marquardt (LM) nonlinear least squares method.

RESULTS

Evolutionary Relationships within the Peroxidase-Cyclooxygenase Superfamily—Here, we have reconstructed the evolutionary lines of the two unexplored bacterial subfamilies within the peroxidase-cyclooxygenase superfamily with 140 full-length protein-coding sequences. The maximum likelihood method of the MEGA 5.05 package (10) was applied with 100 bootstrap replications. The resulting reconstructed phylogenetic tree (Fig. 1) revealed the following: (i) that short bacterial peroxicins form the basal clade of the whole peroxidase-cyclooxygenase superfamily from which all other subfamilies evolved and (ii) that from the peroxidockerins (subfamily 6, highlighted in *blue* in Fig. 1) a direct evolutionary line leads to the well known mammalian peroxidases (subfamily 1). From subfamily 6, the model metalloenzyme for this study was selected. As Fig. 1 demonstrates, the putative peroxidase from the cyanobacterium *Lyngbya* sp. PCC 8106 (LspPOX) clearly belongs to this clade where peroxidockerins and related peroxidases are included (Fig. 1, *blue part*). However, the *Lyngbya* protein does not contain the extra peroxidockerin domain and is closely related to the other short cyanobacterial peroxidases that seemed to have evolved through gene duplication and to have lost the peroxidockerin domain during evolution.

Structural Alignment—Protein sequences used in the evolutionary analysis were taken for structural alignment based on

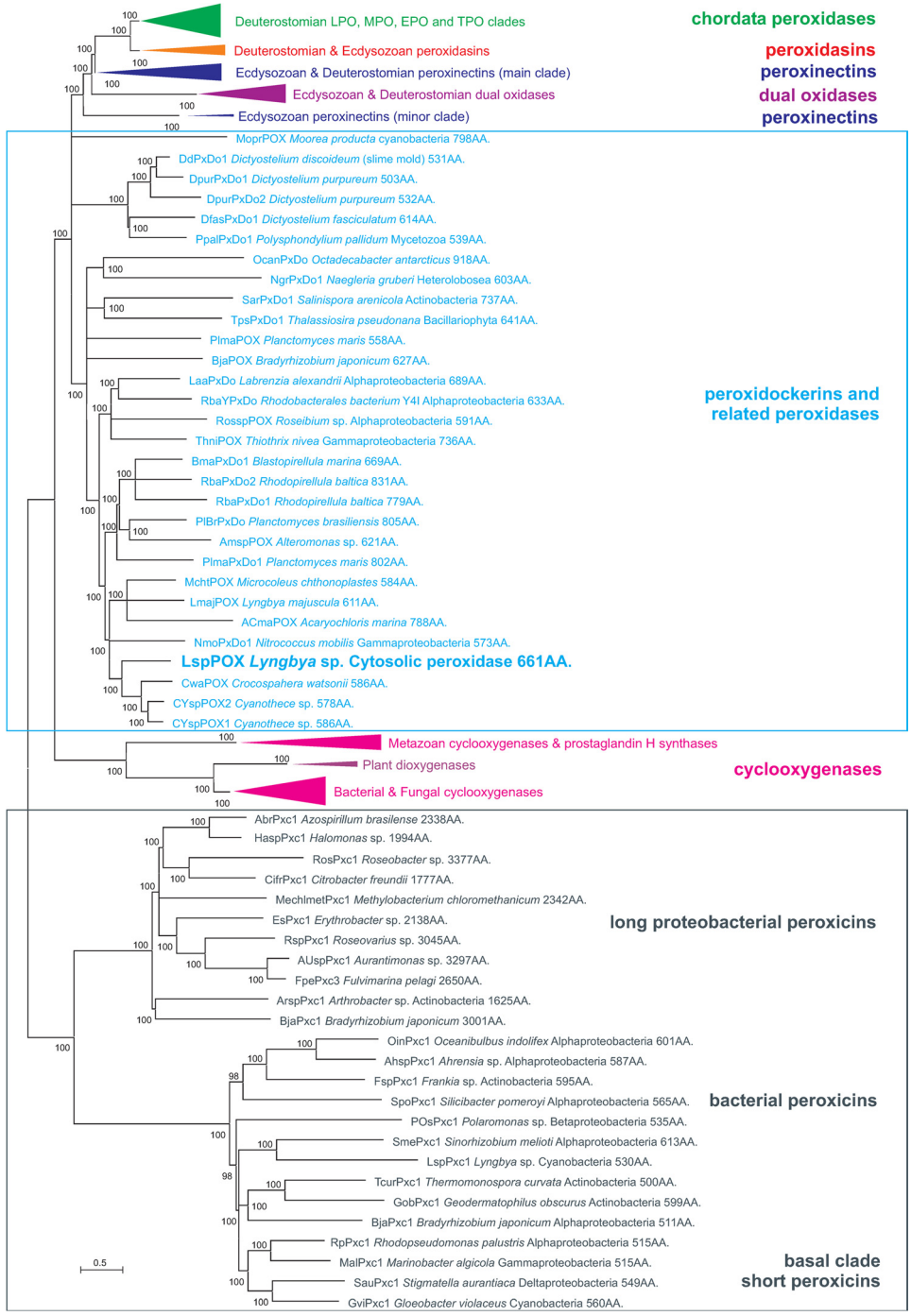

FIGURE 1. **Reconstructed unrooted tree of 140 full-length protein sequences from the peroxidase-cyclooxygenase superfamily.** Molecular phylogeny was inferred using the maximum likelihood method of the MEGA 5.05 package (10). The percentage of replicate trees in which the associated sequences clustered together in the bootstrap test (100 replicates) are shown next to the branches. The tree is drawn to scale, with branch lengths in the same units as those of the evolutionary distances used to infer the phylogenetic tree. Abbreviations of sequence names correspond with PeroxiBase (12).

the known three-dimensional structure of bovine lactoperoxidase (13). With the ESPript program suite, a similarity score for each involved residue was calculated, and the secondary structure elements could be assigned to the corresponding positions. A high level of conservation is seen both on the distal (Fig. 2, *A* and *B*) and on the proximal heme side (Fig. 2*C*). The α-helix α2 harboring the crucial distal catalytic residues His (heterolytic cleavage of H–O–O–H) and Gln (halide binding) as well as the two Asp residues involved in heme and Ca^{2+} binding (4) in LPO are invariantly conserved in all analyzed bacterial peroxidockerins. There is only a small variation regarding the distal Asp residues found in *Rhodopirellula baltica*. This planctomycete has two peroxidockerins, one with the sequence Q*XX*DHD*X* like in LPO, and the second one has both acidic residues exchanged by Ile and Asn (Fig. 2*A*). In the peroxidockerin pseudogene from *Dictyostelium discoideum,* the same variations were found. The other four residues responsible for Ca^{2+} binding (typically located in a loop at the beginning of helix α5) are

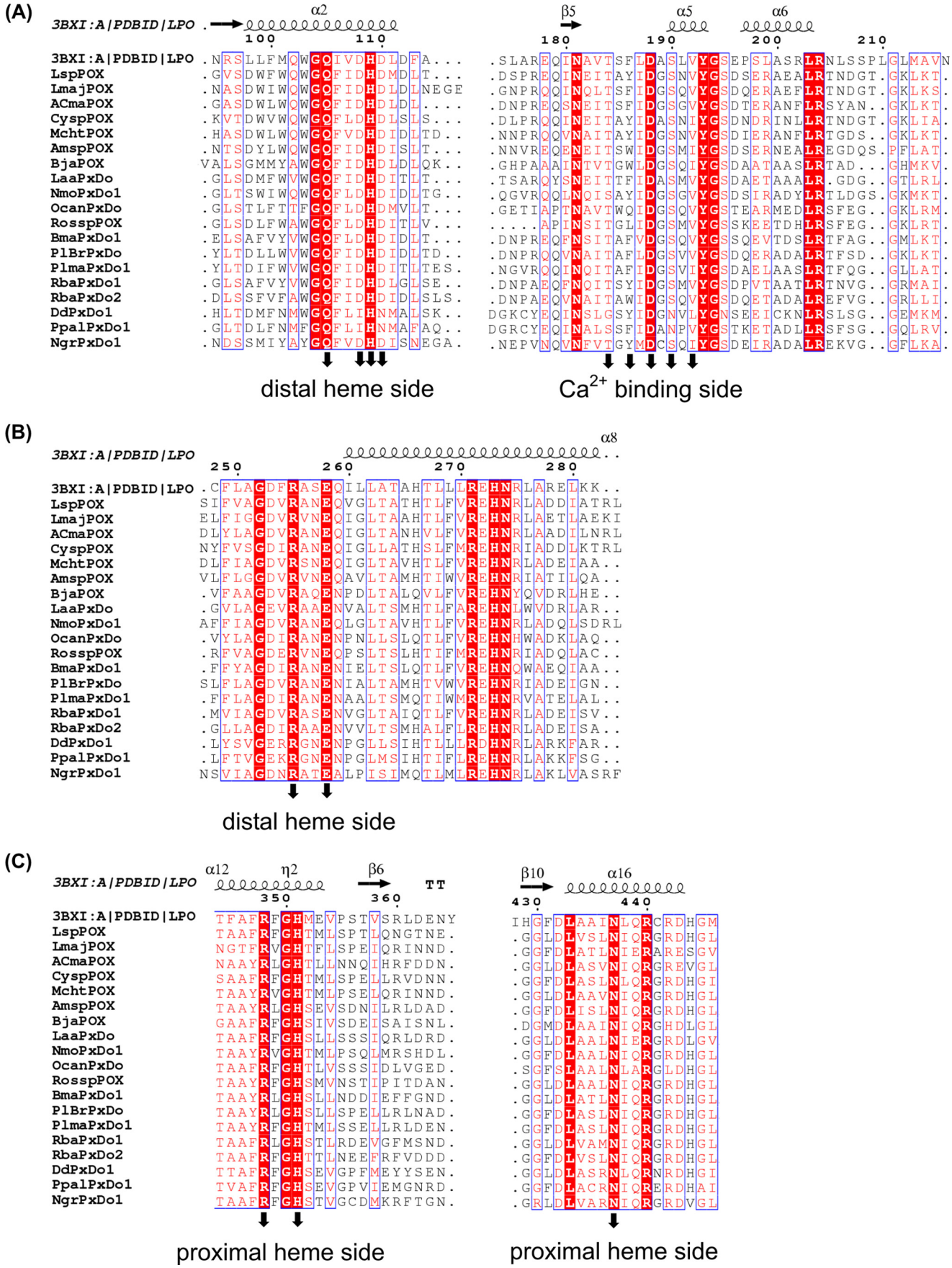
(A)
3BXI:A|PDBID|LPO
α2
β5
α5
α6
100
110
180
190
200
210
3BXI:A|PDBID|LPO .NRSLLFMQWGQQIVDHDLDFA...
LspPOX .GVSDWFWQWGQFIDHDMDLT...
LmajPOX .NASDWIWQWGQFIDHDLDLNEGE
ACmaPOX .GASDWLWQWGQFIDHDLDL....
CyspPOX .KVTDWVWQWGQFLDHDLSLS...
MchtPOX .HASDWLWQWGQFVDHDIDLTD..
AmspPOX .NTSDYLWQWGQFIDHDISLT...
BjaPOX VALSGMMYAWGQFIDHDLDLQK..
LaaPxDo .GLSDMFWVWGQFIDHDITLT...
NmoPxDo1 .GLTSWIWQWGQFLDHDIDLTG..
OcanPxDo .GLSTLFTTFGQFLDHDMVLT...
RosspPOX .GLSDLFWAWGQFIDHDITLV...
BmaPxDo1 .ELSAFVYVWGQFLDHDIDLT...
PlBrPxDo .YLTDLLWVWGQFIDHDIDLTD..
PlmaPxDo1 .YLTDIFWVWGQFIDHDITLTES.
RbaPxDo1 .GLSAFVYVWGQFIDHDLGLSE..
RbaPxDo2 .DLSSFVFAWGQFIDHDIDLSLS.
DdPxDo1 .HLTDMFNMWGQFLIHNMALSK..
PpalPxDo1 .GLTDLFNMFGQFLIHNMAFAQ..
NgrPxDo1 .NDSSMIYAYGQFVDHDISNEGA.
.SLAREQINAVTSFLDASLVYGSEPSLASRLRNLSSPLGLMAVN
.DSPREQINEITAYIDGSNVYGSDSERAEALRTNDGT.GKLKT.
.GNPRQQINQLTSFIDGSQVYGSDQERAEFLRTNDGT.GKLKS.
.DNPREQSNEITSFIDGSGVYGSDTERANFLRSYAN..GKLKT.
.DLPRQQINEITAYIDASNIYGSDNDRINLLRTNDGT.GKLIA.
.NNPRQQVNAITAYIDGSNVYGSDIERANFLRTGDS..GKLKT.
.NNVREQENEITSWIDGSMIYGSDSERNEALREGDQS.PFLAT.
.GHPAAAINTVTGWLDGSQIYGSDAATAASLRTAD...GHMKV.
.TSARQYSNEITTFIDASMVYGSDAETAAALR.GDG..GTLRL.
.QGVRQQLNQISAYIDGSGVYGSDSIRADYLRTLDGS.GKMKT.
.GETIAPTNAVTWQIDGSQVYGSTEARMEDLRSFEG..GKLRM.
.....APINSITGLIDGSMVYGSSKEETDHLRSFEG..GKLRT.
.DNPREQFNSITAFVDGSQVYGSSQEVTDSLRTFAG..GMLKT.
.DNPRQQVNAITAFLDGSVVYGSDQERADALRTFSD..GKLKT.
.NGVRQQINQITAFIDGSVIYGSDAELAASLRTFQG..GLLAT.
.DNPAEQFNQITSYIDGSMVYGSDPVTAATLRTNVG..GRMAI.
.DNPAEQVNAITAWIDGSQVYGSDQETADALREFVG..GRLLI.
DGKCYEQINSLGSYIDGNVLYGNSEEICKNLRSLSG..GEMKM.
DGRCYEQINALSSFIDANPVYGSTKETADLLRSFSG..GQLRV.
.NEPVNQVNFVTGYMDCSQIYGSDEIRADALREKVG..GFLKA.
distal heme side
Ca2+ binding side
(B)
3BXI:A|PDBID|LPO
α8
250
260
270
280
3BXI:A|PDBID|LPO .CFLAGDFRASEQILLATAHTLLLREHNRLARELKK..
LspPOX SIFVAGDVRANEQVGLTATHTLFVREHNRLADDIATRL
LmajPOX ELFIGGDVRVNEQIGLTAAHTLFVREHNRLAETLAEKI
ACmaPOX DLYLAGDVRANEQIGLTANHVLFVREHNRLAADILNRL
CyspPOX NYFVSGDIRANEQIGLLATHSLFMREHNRIADDLKTRL
MchtPOX DLFIAGDVRSNEQIGLTAVHTLFVREHNRLADEIAA..
AmspPOX VLFLGGDVRVNEQAVLTAMHTIWVREHNRIATILQA..
BjaPOX .VFAAGDVRAQENPDLTALQVLFVREHNYQVDRLHE..
LaaPxDo .GVLAGEVRAAENVALTSMHTLFAREHNLWVDRLAR..
NmoPxDo1 AFFIAGDVRANEQLGLTAVHTLFVREHNRLADQLSDRL
OcanPxDo .VYLAGDIRANENPNLLSLQTLFVREHNHWADKLAQ..
RosspPOX .RFVAGDERVNEQPSLTSLHTIFMREHNRIADQLAC..
BmaPxDo1 .FFYAGDIRANENIELTSLQTLFVREHNQWAEQIAA..
PlBrPxDo SLFLAGDVRANENIALTAMHTVWVREHNRIADEIGN..
PlmaPxDo1 .FFLAGDIRANENAALTSMQTIWMREHNRVATELAL..
RbaPxDo1 .MVIAGDVRASENVGLTAIQTLFVREHNRLADEISV..
RbaPxDo2 .GLLAGDIRAAENVVLTSMHALFLREHNRLADEISA..
DdPxDo1 .LYSVGERRGNENPGLLSIHTLLLRDHNRLARKFAR..
PpalPxDo1 .LFTVGEKRGNENPGLMSIHTIFLREHNRLAKKFSG..
NgrPxDo1 NSVIAGDNRATEALPISIMQTLMLREHNRLAKLVASRF
distal heme side
(C)
3BXI:A|PDBID|LPO
α12
η2
β6
TT
350
360
β10
α16
430
440
3BXI:A|PDBID|LPO TFAFRFGHMEVPSTVSRLDENY
LspPOX TAAFRFGHTMLSPTLQNGTNE.
LmajPOX NGTFRVGHTFLSPEIQRINND.
ACmaPOX NAAYRLGHTLLNNQIHRFDDN.
CyspPOX SAAFRFGHTMLSPELLRVDNN.
MchtPOX TAAYRVGHTMLPSELQRINND.
AmspPOX TAAYRLGHSEVSDNILRLDAD.
BjaPOX GAAFRFGHSIVSDEISAISNL.
LaaPxDo TAAFRFGHSLLSSSIQRLDRD.
NmoPxDo1 TAAYRVGHTMLPSQLMRSHDL.
OcanPxDo TAAFRFGHTLVSSSIDLVGED.
RosspPOX TAAYRFGHSMVNSTIPITDAN.
BmaPxDo1 TAAYRLGHSLLNDDIEFFGND.
PlBrPxDo TAAYRLGHSLLSPELLRLNAD.
PlmaPxDo1 TAAYRFGHTMLSSELLRLDEN.
RbaPxDo1 TAAFRLGHSTLRDEVGFMSND.
RbaPxDo2 TAAFRFGHTTLNEEFRFVDDD.
DdPxDo1 TTAFRFGHSEVGPFMEYYSEN.
PpalPxDo1 TVAFRFGHSEVGPVIEMGNRD.
NgrPxDo1 TAAFRFGHSTVGCDMKRFTGN.
IHGFDLAAINLQRCRDHGM
.GGLDLVSLNIQRGRDHGL
.GGFDLATLNIERARESGV
.GGLDLASVNIQRGREVGL
.GGFDLASLNLQRGRDHGI
.GGLDLAAVNIQRGRDHGL
.GGFDLISLNIQRGRDHGL
.DGMDLAAINIQRGHDLGL
.GGLDLAALNIERGRDLGV
.GGFDLAALNIQRGRDHGL
.SGFSLAALNLARGLDHGL
.GGLDLAALNIQRGRDHGL
.GGLDLATLNIQRGRDHGL
.GGFDLASLNIQRGRDHGL
.GGFDLASLNIQRGRDHGL
.GGLDLVAMNIQRGRDHGL
.GGFDLVSLNIQRGRDHGL
.GGLDLASRNLQRNRDHGI
.GGFDLACRNIQRERDHAI
.GRLDLVARNIQRGRDVGL
proximal heme side
proximal heme side

also conserved in all short peroxidockerins except from *R. baltica* and *D. discoideum* (Fig. 2*A*, *right panel*). The distal catalytic Arg and neighboring Glu (involved in second heme to protein link in LPO) are invariantly conserved in the region before the long helix α8 (Fig. 2*B*). On the proximal side, two α-helices (α12 and α16) bearing the essential proximal His with its hydrogen bonding partner Asn are also found in all sequenced representatives of this clade (Fig. 2*C*).

This analysis led us to the conclusion that the active site architecture of halogenating heme peroxidases is evolutionarily strongly preserved. Next, we wanted to investigate whether this high homology between the peroxidase from *Lyngbya* sp. (LspPOX) and the mammalian lactoperoxidase is also reflected by the biochemical and biophysical properties of this new bacterial metalloprotein.

Spectral Properties of Ferric and Ferrous LspPOX—Recombinant LspPOX has been purified to homogeneity. The average yield varied between 6 and 11 mg/liter *E. coli* culture. Size-exclusion chromatography (data not shown) clearly demonstrated that the 59-kDa protein was monomeric with purity numbers ($A_{412\ nm}/A_{280\ nm}$) ranging from 0.90 to 0.92 that reflected almost 100% heme occupancy. Mass spectrometric analysis showed that in the recombinant protein isoleucine is the N-terminal amino acid. The theoretical average neutral mass without a prosthetic group was determined by mass spectrometry to be 59.4 kDa (see below). The full amino acid sequence of the recombinant protein is depicted in Fig. 5*E*.

It was interesting to see that LspPOX exhibited spectral properties similar to bovine LPO that has a modified and covalently bound heme group (4). The ferric mammalian protein has its Soret band at 412 nm and further peak maxima at 501, 545, 587, and 631 nm (Fig. 3*B*) (23). Recombinant LspPOX exhibits similar spectral properties with maxima at 412, 501, 545, 587, 641, and 662 nm (Figs. 3*C* and 4*C*). For comparison, ferric HRP (that has a nonmodified heme *b*) has its Soret band at 402 nm and further maxima at 503 and 641 nm (Fig. 3*A*). These data indicated that the spectral properties of LspPOX are LPO-like and that its prosthetic group experienced a different coordination and/or environment than in HRP.

We soon realized that the biophysical and biochemical properties of the bacterial protein were modified upon addition of micromolar concentrations of hydrogen peroxide. For this reason, we always compare recombinant LspPOX as it is produced by *E. coli* with the protein preincubated with a stoichiometric excess of hydrogen peroxide, which we now designate LspPOX (H_2O_2). In most of the investigations, a 15 times molar excess of H_2O_2 was used for incubation of LspPOX. As will be shown below, peroxide treatment increased the homogeneity of the protein by triggering the formation of covalent heme to protein bonds.

In the beginning, we probed the kinetics of spectral transition of reduction of the ferric proteins by dithionite. Again HRP and LPO were used as reference proteins with known three-dimensional structures. The reactions were studied by conventional stopped-flow spectroscopy. In the case of HRP, there was a simple and clear direct transition from the ferric state (402, 503, and 641 nm) to the ferrous state (436, 558, and 587 nm) with a clear isosbestic point at 419 nm within 10 s at pH 7.0 (Fig. 3*A*). By contrast, upon using the same amount of dithionite (*i.e.* 24 mM) for reduction of ferric LPO, a transient intermediate with a Soret maximum at 447 nm and additional bands in the visible region at 563 and 596 nm was formed immediately within 120 ms (isosbestic point at 428 nm). This species was not stable and converted slowly but completely within 400 s to a stable form with a Soret maximum at 432 nm (isosbestic point at 440 nm) (Fig. 3*B*). Concomitantly the peak at 596 nm lost absorbance. Upon reduction of ferric LspPOX with dithionite, it was directly transformed to a transient intermediate state (447, 560, and 594 nm) within 5 s (isosbestic point at 425 nm) that was slowly converted to the stable ferrous form with a Soret band at 432 nm and a more pronounced absorbance at 560 nm (isosbestic point at 442 nm) (Fig. 3*C*).

Fig. 4*A* clearly demonstrates that LspPOX and LspPOX (H_2O_2) have the identical secondary structure content. Differences were only seen in the active site architecture as it is reflected by the ECD spectra of both forms in the visible region (Fig. 4*B*). Moreover, comparing the UV-visible spectra in the visible region of the resting state of LspPOX with that of LspPOX (H_2O_2) showed that upon H_2O_2 treatment the Soret band was sharpened and shifted to 413 nm. Concomitantly, the absorbance at the Soret maximum decreased by about 13%. The *inset* to Fig. 4*C* depicts the difference in the UV-visible spectrum of LspPOX and LspPOX (H_2O_2).

Upon reduction of ferric LspPOX (H_2O_2), the intermediate state with peaks at 447, 563, and 596 nm was formed within 1 s. In contrast to both LspPOX and LPO, it remained relatively stable. Its conversion to the state with a Soret maximum at 440 nm occurred very slowly (isosbestic point at 430 nm) (Fig. 3*D*).

EPR Spectroscopy—The continuous wave of EPR spectra of LspPOX and LspPOX (H_2O_2) in comparison with LPO is depicted in Fig. 4*D*. The spectrum of LspPOX showed the presence of three rhombically distorted high spin form(s), arising from the transition of $m_s = \pm ½$ of an $S = 5/2$ system. The rhombicity η (E/D, where D is the axial and E the rhombic distortion) varied between 0.007 and 0.033 (Table 1). About 70% of the high spin moiety was characterized by a rhombicity of 0.023 (Fig. 4*D*). Upon preincubation with H_2O_2, the low field range of the EPR spectrum visibly changed and became similar to the spectrum of LPO. Based on spectral simulation, four high spin compounds were formed in LspPOX (H_2O_2) where more than 60% had a rhombicity between 0.014 and 0.019 (Table 1), which is lower than the major rhombic coordination in LspPOX. This is close to the high spin compound found in LPO ($\eta = 0.018$, see Fig. 4*D* and Table 1). The change in the rhom-

FIGURE 2. **Structural alignment of different peroxidockerins with lactoperoxidase.** ESPript output was obtained from 20 sequences homologous to 3BXI. Secondary structure elements are presented on the *top* of the alignment as follows: helices with *squiggles*, β-strands with *arrows*, and turns with *TT* letters. Conserved residues are written in *red* within sequence blocks. Abbreviations of sequences correspond with PeroxiBase (12). Important residues are marked by *arrows*. *Numbering* corresponds to bovine lactoperoxidase. *A,* conserved distal regions, including the catalytic His and Gln (halide binding) and two Asp (heme to protein bond and Ca^{2+} binding); *B,* catalytic Arg and Glu (heme to protein bond), and *C,* conserved proximal region, including the proximal His and its H-bonding partner Asn.

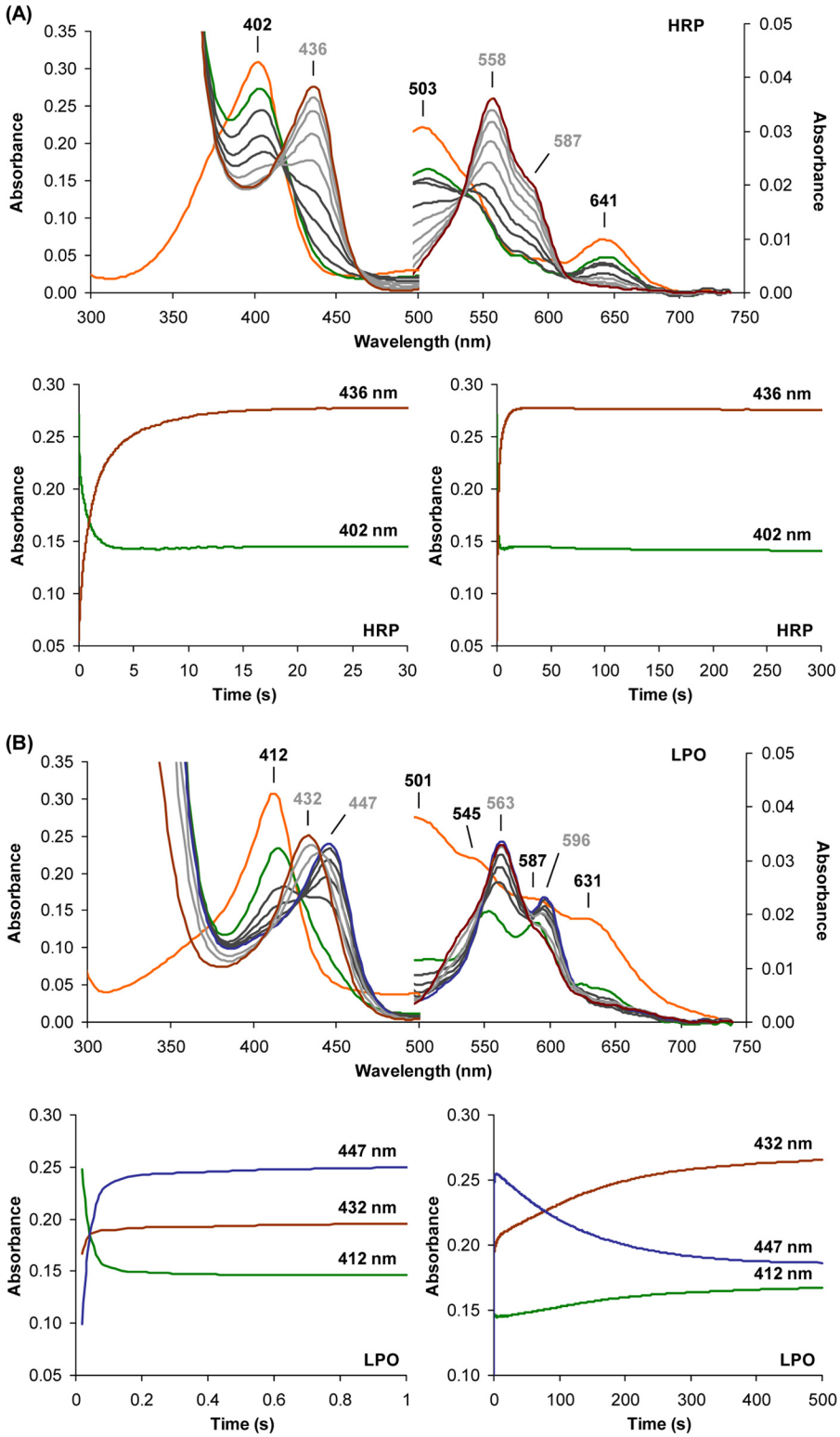

FIGURE 3. **Kinetics of spectral transition of ferric to ferrous state of heme peroxidase from *Lyngbya* PCC 8106 in comparison with HRP and LPO.** *A,* spectral transition upon mixing 4 μM ferric horseradish peroxidase with 24 mM dithionite in 10 mM phosphate buffer, pH 7.0, by using the conventional stopped-flow spectroscopy. The first spectrum was taken 19 ms after mixing (*green line*) (25 °C). For comparison, the ferric spectrum of HRP is inserted and depicted in *orange*. *B,* spectral transition upon mixing of 4 μM ferric bovine LPO with 24 mM dithionite in 10 mM phosphate buffer, pH 7.0, by using the conventional stopped-flow spectroscopy. The first spectrum was taken 19 ms after mixing (*green line*) (25 °C). For comparison, the ferric spectrum of LPO is inserted and depicted in *orange*. *C,* spectral transition upon mixing of 4 μM ferric LspPOX with 24 mM dithionite in 10 mM phosphate buffer, pH 7.0, by using the conventional stopped-flow spectroscopy. The first spectrum was taken 19 ms after mixing (*green line*) (25 °C). *D,* spectral transition upon mixing of 4 μM ferric LspPOX (H_2O_2) with 24 mM dithionite in 10 mM phosphate buffer, pH 7.0, by using the conventional stopped-flow spectroscopy. The first spectrum was taken 19 ms after mixing (*green line*) (25 °C). In all examples, the corresponding time traces at defined Soret maxima of the various conformers are shown.

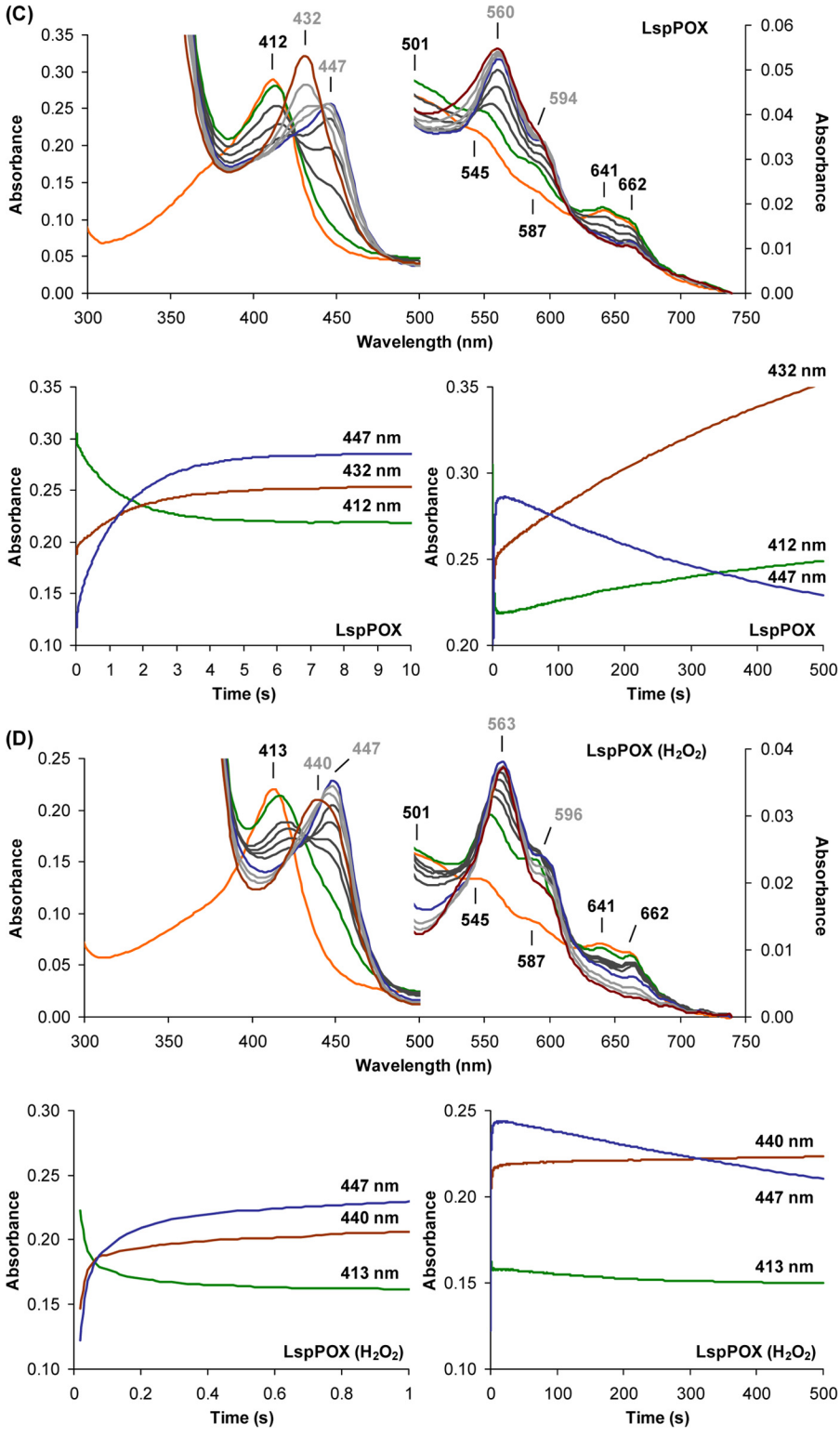

FIGURE 3—*Continued*

bicity in LspPOX (H_2O_2) in comparison with LspPOX indicates a rearrangement around the heme center of the enzyme toward axial symmetry. Still, there were several conformations present in LspPOX (H_2O_2), which might be explained because the autocatalytic process was not fully completed and left some protein fractions without or only partial covalently linked heme.

Evidence of Covalently Bound Heme in LspPOX (H_2O_2)—In the beginning, protein denaturation and precipitation by acidic acetone were probed to analyze the interaction between the prosthetic group and the protein. Upon precipitation of LspPOX (H_2O_2) and LPO, the supernatant remained colorless, whereas the pellet was colored. With HRP and LspPOX, the

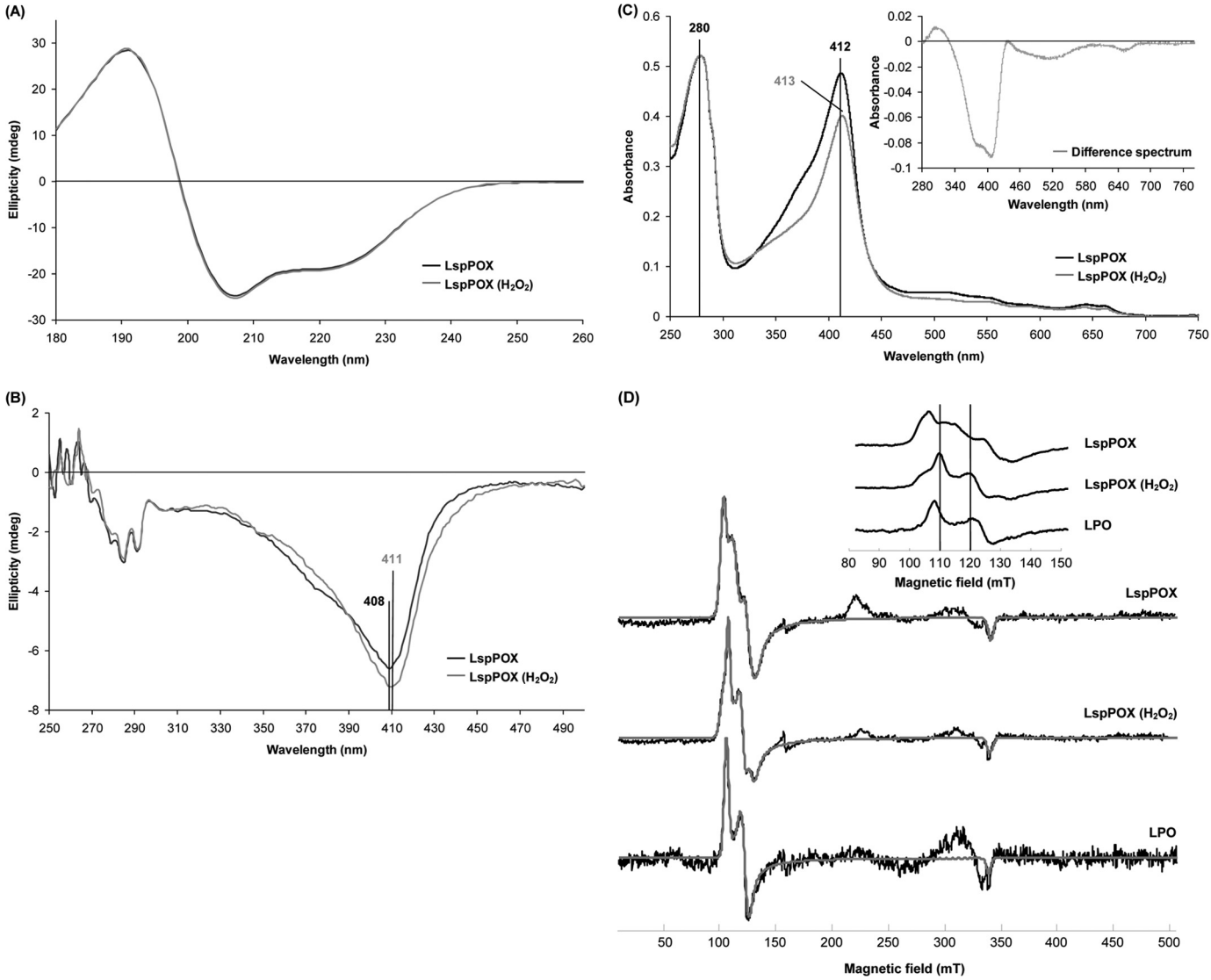

FIGURE 4. **ECD, UV-visible, and continuous wave electron paramagnetic resonance spectra of heme peroxidase from *Lyngbya* PCC 8106.** *A* and *B,* circular dichroism spectra of *Lyngbya* PCC 8106. *A,* far-UV ECD spectra of LspPOX and LspPOX (H_2O_2) pretreated with the 15 times molar excess of hydrogen peroxide for 1 h and room temperature. *B,* near-UV and visible ECD spectra of LspPOX and LspPOX (H_2O_2) pretreated with the 15 times molar excess of hydrogen peroxide. Enzyme concentration of LspPOX and LspPOX (H_2O_2) was identical. *C,* UV-visible spectra of LspPOX and LspPOX (H_2O_2), including the difference spectrum. *D,* experimental continuous wave EPR spectra (*black*) and simulations of their high spin compounds (*gray*) of LspPOX, LspPOX (H_2O_2), and bovine LPO at pH 7.0 and 10 K. The *inset* shows the low field region of the spectra. *Vertical lines* in the *inset* support the visibility of changes between the individual spectra.

TABLE 1

EPR simulation parameters (effective *g* values and rhombicity *E/D*) of the low temperature EPR spectra of LspPOX, LspPOX (H_2O_2), and LPO (HS, high spin)

Simulations were carried out using EasySpin (41).

Sample	g_x^{eff}	g_y^{eff}	g_z^{eff}	*E/D*
LspPOX				
HS1	5.80	6.11	2.00	0.007
HS2	5.40	6.50	1.99	0.023
HS3	5.15	6.70	1.98	0.033
LspPOX (H_2O_2)				
HS1	5.80	6.11	2.00	0.007
HS2	5.60	6.27	1.99	0.014
HS3	5.52	6.40	1.99	0.019
HS4	5.28	6.60	1.98	0.028
LPO				
HS	5.52	6.40	2.00	0.018

supernatant contained free heme (maximum around 384 nm), and the precipitated protein was (almost) colorless (Fig. 5*A*). These data clearly suggested that hydrogen peroxide triggered covalent binding of the prosthetic group in LspPOX.

This was verified by mass spectrometric analysis of the intact protein that has a theoretical average neutral mass without prosthetic group of 59,402 Da (Fig. 5, *B* and *C*). When heme *b* is bound to the protein LspPOX (H_2O_2), a mass increment of 612 Da must be added. It must be noted that during the sample preparation for mass spectrometry, noncovalently bound heme was completely lost due to protein unfolding. Analysis of LspPOX showed that about 80% of the protein was heme-free (Fig. 5*B*). However, upon incubation with 15 times molar excess of hydrogen peroxide, the mass peak at 60,014 Da (Fig. 5*C*) dominated representing about 71% heme-linked protein.

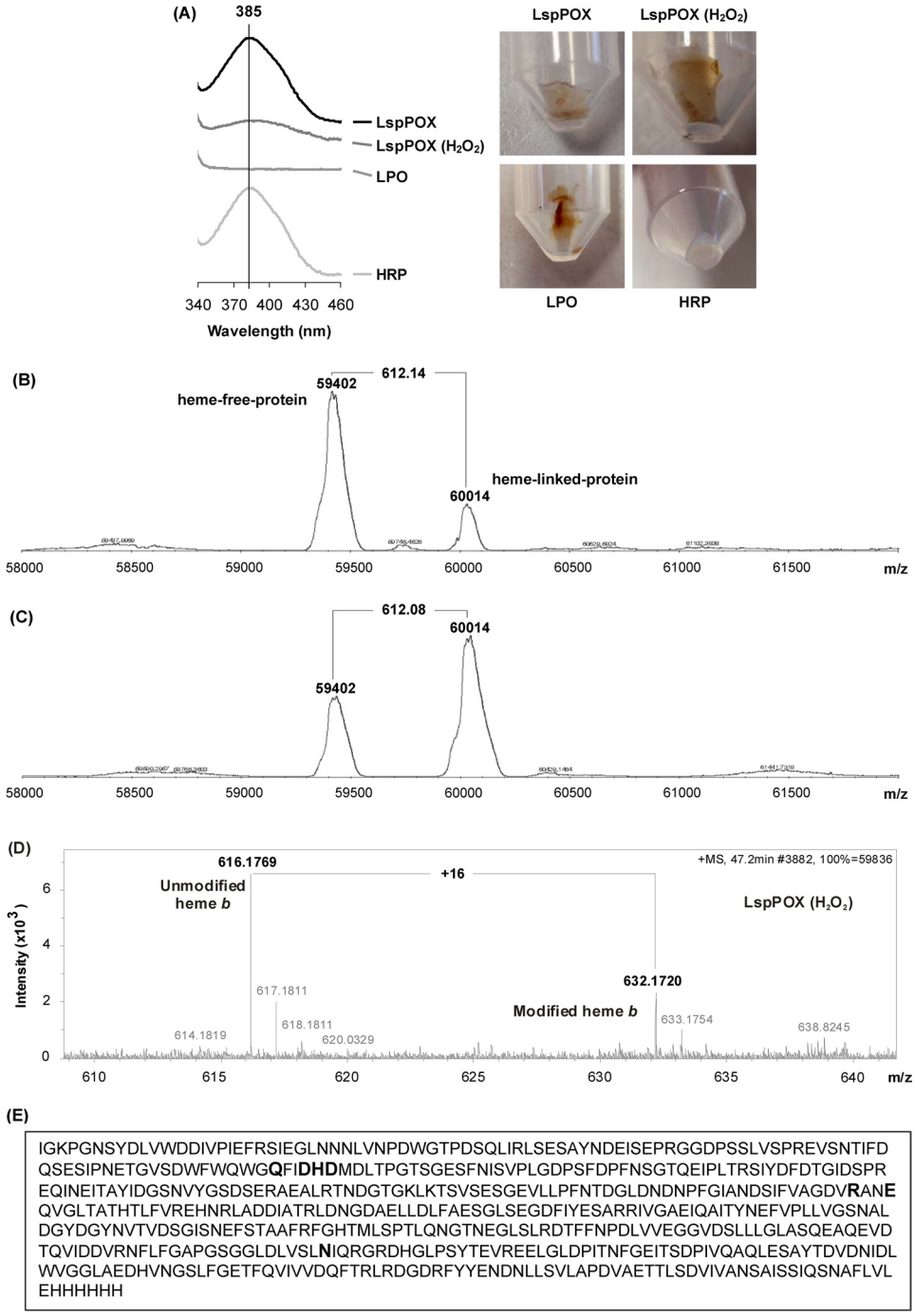

FIGURE 5. **Mass spectrometric analysis of heme peroxidase from *Lyngbya* PCC 8106.** *A,* acetone precipitation of LspPOX, LspPOX (H_2O_2), LPO, and HRP. Acetone precipitation (addition of 7-fold volume of acetone) of the four protein samples and analysis of supernatant and precipitated protein. *B* and *C,* MS analysis of LspPOX (*B*) in comparison with LspPOX (H_2O_2) (*C*). *D,* MS analysis of prosthetic group of LspPOX (H_2O_2). The enzyme was incubated by GluC/trypsin, and the digest was strongly acidified. The obtained pellet was solved by neutralization and analyzed by LC-MS. *E,* in addition the amino acid sequence of the recombinant protein is shown (molar mass without heme 59,402 Da). Highly conserved distal and proximal heme residues are depicted in *bold*; compare with Fig. 2).

Next, we have digested both LspPOX and LspPOX (H_2O_2) by GluC/trypsin and analyzed the resulting peptides by LC-MS analysis. Because we did not succeed in finding a heme-linked peptide, we compared the ratios of the peak areas of the respective peptides found after digestion of LspPOX and LspPOX (H_2O_2). Table 2 demonstrates that these ratios were very similar for all selected peptides (1.6–1.85) except for one that contained a glutamate. Sequence alignment with LPO (Fig. 2*B*) suggested that this acidic residue (Glu-229) could be involved in the formation of an ester linkage with the modified heme group. In LspPOX (H_2O_2), in contrast to LspPOX, this peptide was bound to the prosthetic group that significantly changed the peptide ratio to 3.03. Simultaneously, the ratio of noncovalently bound heme increased to the same extent (Table 2).

Finally, we analyzed the pellet obtained by acidification of the protein digest. After centrifugation, the precipitate was solved

TABLE 2

Digestion of LspPOX and LspPOX (H_2O_2) by GluC/trypsin and analysis by LC-MS

MS data from 10 peptides and heme *b* are depicted, and the ratio of the respective peak areas are given as LspPOX/LspPOX (H_2O_2). Peptides 2 and 3 include those acidic amino acids (boldface) that have been proposed to be involved in heme binding. BPC, base peak chromatogram.

number	peak area LspPOX	LC-MS signal	peak area LspPOX (H_2O_2)	ratio LspPOX/LspPOX (H_2O_2)	sequence	charge	note
1	11339079	BPC 616.17±0.05	3767779	**3.01**	**heme**	1	heme *b*
2	8885509	BPC 878.97±0.05	2936081	**3.03**	AN**E**QVGLTATHTLFVR	2	E229
3	5227940	BPC 1038.11±0.05	2796607	**1.87**	TGVSDWFWQWGQFI**D**HDMDLTPGTSGE	3	D100
4	162637558	BPC 743.34±0.05	101644950	1.60	SIYDFDTGIDSPR	2	randomly chosen peptides
5	111792171	BPC 437.73±0.05	60543473	1.85	LADDIATR	2	
6	86927598	BPC 725.72±0.05	49219881	1.77	NFLFGAPGSGGLDLVSLNIQR	3	
7	19253401	BPC 634.78±0.05	10911863	1.76	EVSNTIFDQS E	2	
8	1616010	BPC 785.69±0.05	918654	1.76	SFNISVPLGD PSFDPFNSGT QE	3	
9	5771327	BPC 904.91±0.05	3330406	1.73	EVSNTIFDQS ESIPNE	2	
10	7567114	BPC 1218.20±0.05	4327257	1.75	TFQVIVVDQFTR	2	
11	47404493	BPC 657.35±0.05	28280927	1.68	ITSDPIVQAQLE	2	

upon neutralization and analyzed by LC-MS. Fig. 5*D* depicts the occurrence of a heme species with an *m*/*z* value of 632.17, which indicates that one methyl substituent of heme *b* was converted to hydroxymethyl in LspPOX (H_2O_2).

Redox Chemistry of LspPOX—Fig. 6 shows the spectral transition upon reduction of untreated and H_2O_2-treated ferric LspPOX at different applied potentials in the OTTLE cell (25 °C, pH 7) along with the corresponding Nernst plots. Because, as demonstrated above, reduction of ferric LspPOX proceeds through the formation of a transient ferrous intermediate (Fig. 3*C*), LspPOX was first fully reduced electrochemically. This allowed complete conversion into its stable ferrous form (432 nm), which was then subjected to (oxidative) spectroelectrochemical titrations (Fig. 6). Therefore, the $E^{0\prime}$ values refer to the redox equilibrium between the stable Fe(II) form of LspPOX and the ferric species. The Nernst plot obtained from these electrochemical titrations of LspPOX was linear (*inset* to Fig. 6*A*) and allowed the calculation of $E^{0\prime}$ of the coupled Fe(III)/Fe(II) to be −184 ± 8 mV (25 °C and pH 7.0), which was in the range reported for LPO (−176 and −190 mV) (17, 25).

Next, we have preincubated LspPOX with different amounts of H_2O_2 (9, 15, 18, and 25 times molar excess) for 1 h at room temperature before performing the spectroelectrochemical measurements. In contrast to the untreated protein, the resulting stable Fe(II) spectrum suggested the presence of two conformers with maxima at 434 and 447 nm. The higher the H_2O_2 concentration, the more dominating was the Fe(II) state with the Soret maximum at 447 nm (compare Fig. 6, *B* and *C*). This reflects the stopped-flow data presented above (Fig. 3*D*). The observed reduced forms were electrochemically oxidized, obtaining slightly different $E^{0\prime}$ values, most probably because of the different ratios of the $\text{conformer}_{447\text{ nm}}/\text{conformer}_{434\text{ nm}}$.

In particular, the spectroelectrochemical titration of LspPOX (H_2O_2) obtained upon preincubation with 9 times molar excess of H_2O_2 (Fig. 6*B*) provided an $E^{0\prime}$ of −145 ± 10 mV. This value, which is slightly higher than that of the untreated protein, can be ascribed to the redox equilibrium between the stable Fe(II) form of LspPOX (H_2O_2) and the ferric species, because the spectral properties of electrochemically reduced protein closely match those of the final adduct obtained upon dithionite reduction of LspPOX (H_2O_2) (Fig. 3*D*).

However, the $E^{0\prime}$ obtained from the spectroelectrochemical titration of LspPOX (H_2O_2) preincubated with 25 times molar excess of H_2O_2 (Fig. 6*C*) refers to the Fe(III) → $\text{Fe(II)}_{447\text{ nm}}$ reaction, because only the ferrous $\text{conformer}_{447\text{ nm}}$ is observed in the experimental conditions used. Interestingly, the obtained reduction potential (−160 ± 10 mV) is 15 mV more negative than that of the stable form of LspPOX (H_2O_2), indicating that the structural differences existing between the two ferrous conformers of LspPOX (H_2O_2) affect both the spectroscopic and the redox properties of the heme group. This is an unprecedented finding, because the redox equilibrium between the ferric form of LPO and its transient Fe(II) intermediate was not analyzed due to the short lifetime of the latter species (17).

Enzymatic Activity—It has to be mentioned that in the steady-state kinetic assays, the discrimination between LspPOX and LspPOX (H_2O_2) was not necessary due to the high stoichiometric excess of hydrogen peroxide (50 nM enzyme *versus* 100 μM H_2O_2). Nevertheless, in all enzymatic assays LspPOX (H_2O_2) was used. Fig. 7*A* depicts typical time traces of the formation of TauBr by 100 nM LspPOX (H_2O_2) compared with 100 nM LPO in the presence of 200 μM H_2O_2. Catalysis of the reaction by the bacterial enzyme was finished within 1 s, which is about 10 times faster than by LPO. At pH 7.0, bromination of taurine mediated by LspPOX (H_2O_2) was highest (Fig. 7*B*), whereas the pH optimum of TauBr formation mediated by LPO was at pH 5.5. The same pH-profile was obtained using the adjusted MCD assay (data not shown). The MS data presented in Fig. 7, *E* and *F*, clearly demonstrate that TauBr is produced in these reactions. In the presence of LspPOX (H_2O_2), 500 μM H_2O_2, 5 mM taurine, and 50 mM bromide, the intensity of the taurine peak at $m/z = 124.01$ decreased, and new mass peaks of similar intensity at *m*/*z* of 201.9 and 203.91 appeared, reflecting the occurrence of the two bromine isotopes Br-79 (50.7%) and Br-81 (49.3%) in TauBr.

LspPOX also exhibited a relatively poor chlorination activity. MPO was used as a reference protein, because LPO was not able to oxidize chloride. Fig. 7*C* compares the chlorination activity of taurine of LspPOX (H_2O_2) and MPO. In the neutral region, the bacterial enzyme was unable to oxidize chloride, but by decreasing the pH, the formation of TauCl was slightly increased. This was also demonstrated by MS analysis at pH 5.0,

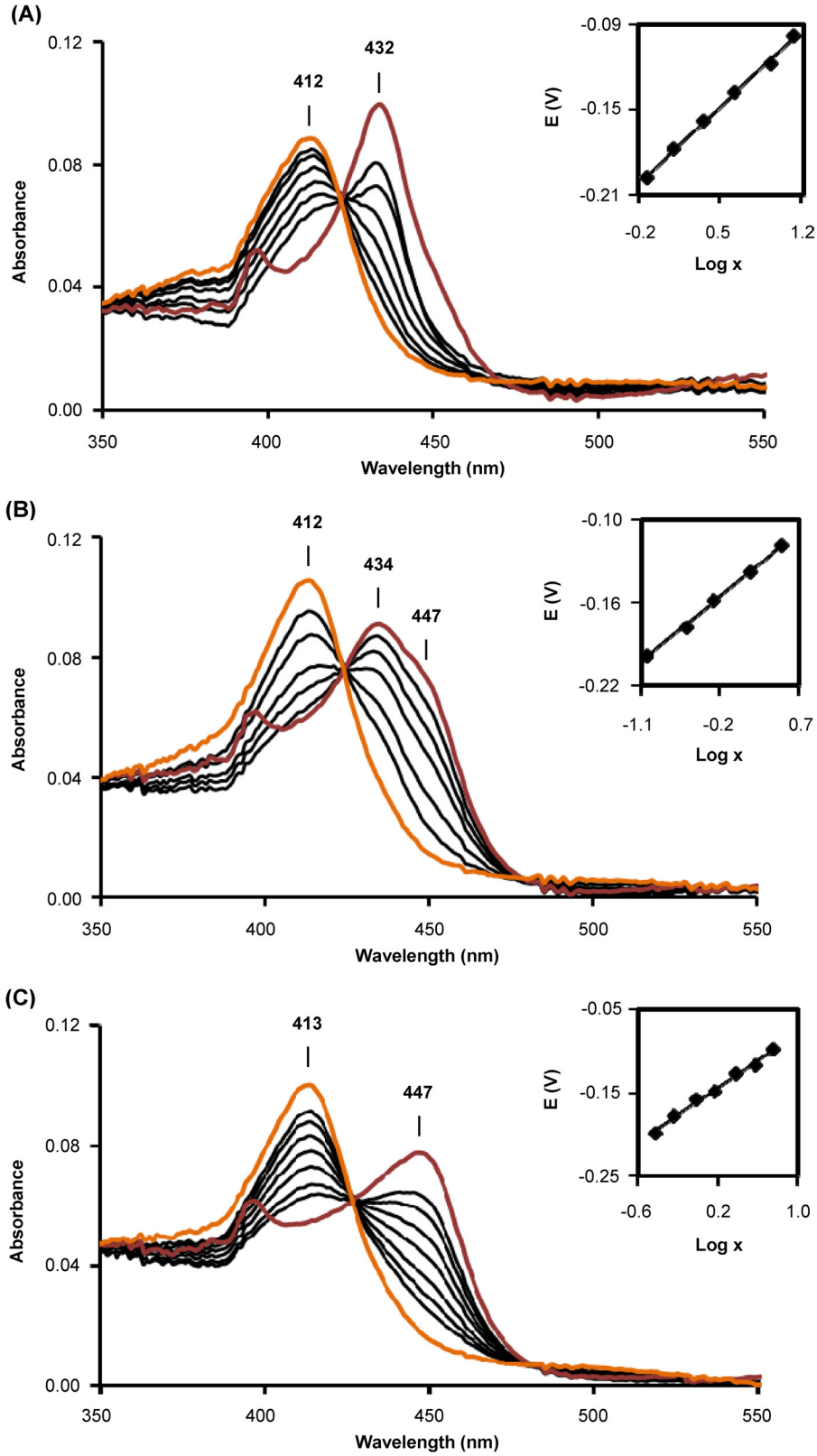

FIGURE 6. **Redox properties of heme peroxidase from *Lyngbya* PCC 8106.** Electronic spectra of recombinant (untreated) LspPOX (*A*) and LspPOX (H_2O_2) (obtained upon incubation of LspPOX for 1 h at room temperature with 9-fold (*B*) and 25-fold (*C*) molar excess of hydrogen peroxide) were recorded at various potentials in spectroelectrochemical experiments carried out with an OTTLE cell at 25 °C, pH 7.0. The corresponding Nernst plots are shown in the *insets*, where *X* stands for $((A_{\lambda red,\,max} - A_{\lambda red})/(A_{\lambda ox,\,max} - A_{\lambda ox}))$. In case of untreated LspPOX, $\lambda_{ox} = 412$ nm and $\lambda_{red} = 432$ nm (*A*); in case of LspPOX (H_2O_2) (obtained upon incubation with 9-fold molar excess of hydrogen peroxide), $\lambda_{ox} = 413$ nm and $\lambda_{red} = 434$ nm (*B*), and for LspPOX (H_2O_2) (obtained upon incubation with 25-fold molar excess of hydrogen peroxide), $\lambda_{ox} = 413$ nm and $\lambda_{red} = 447$ nm (*C*). Spectroelectrochemical titrations were carried out using samples containing 10 μM LspPOX (*A*) or 12 μM LspPOX (H_2O_2) (*B* and *C*) dissolved in 100 mM phosphate buffer and 100 mM NaCl at pH 7.0, in the presence of 80 μM (*A*) or 100 μM (*B* and *C*) methyl viologen and 2 μM of lumiflavin-3-acetate, methylene blue, phenazine methosulfate, and indigo disulfonate used as mediators.

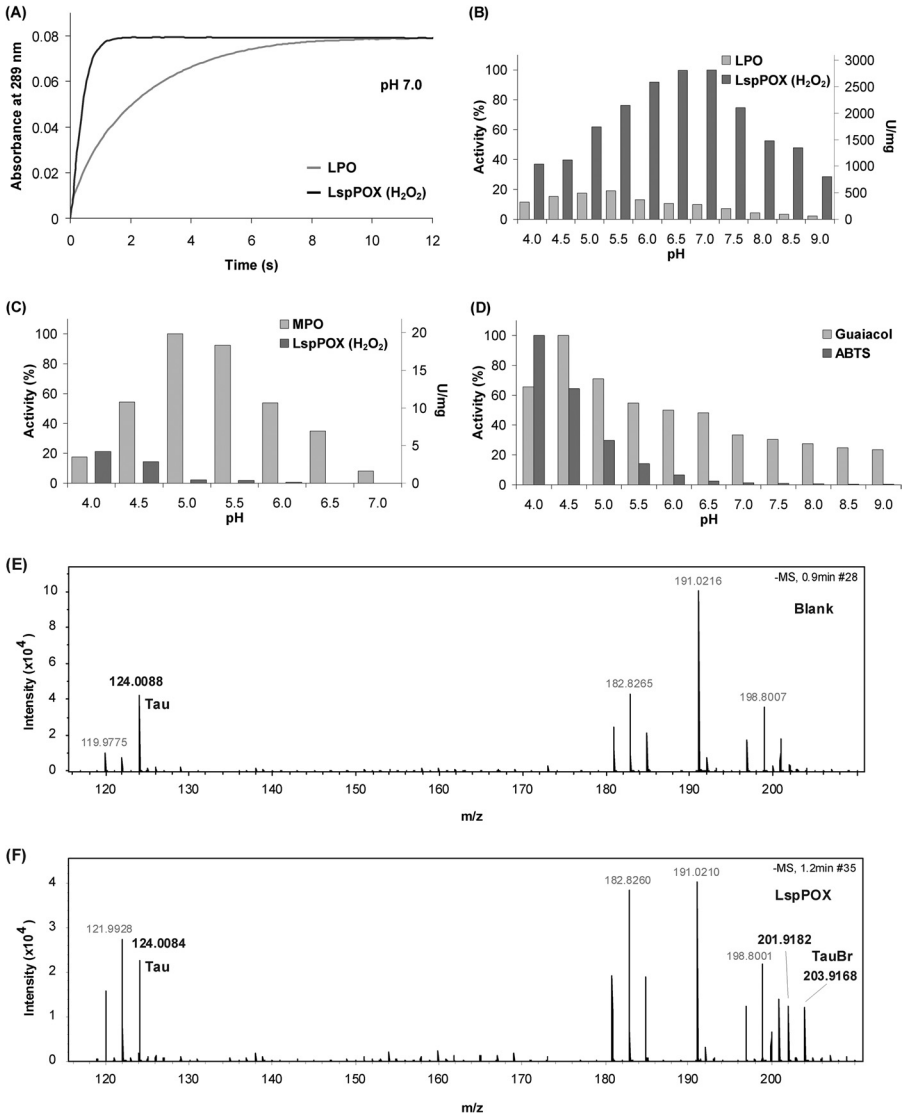

FIGURE 7. **Halogenation and peroxidase activity of the heme peroxidase from *Lyngbya* PCC 8106.** *A,* typical time traces of the formation of taurine bromamine by LspPOX (H_2O_2) in comparison with LPO. Conditions are as follows: 100 nM enzyme, 10 mM taurine, 100 mM KBr, 200 μM H_2O_2, 100 mM phosphate buffer, pH 7.0. *B,* bromination activity of LspPOX in comparison with bovine lactoperoxidase (*LPO*) in the pH range 4.0 to 9.0. Conditions are as in *A* except for usage of different (overlapping) buffer systems. *C,* chlorination activity of LspPOX (H_2O_2) in comparison with human MPO in the pH range 4.0 to 7.0. Conditions are as in *B* except for usage of 100 mM NaCl. *D,* peroxidase activity of LspPOX (H_2O_2) with 100 μM guaiacol or 1 mM μM ABTS in the pH range 4.0 to 9.0. Enzyme used is as follows: 50 nM, H_2O_2, 100 μM. Used buffers are as follows: 100 mM carbonate buffer, pH 8.0–10.0, 100 mM phosphate buffer, pH 5.0–8.0, or 100 mM citrate/phosphate buffer, pH 4.0–5.0. Activity is given in percentage of maximum activity (100%) at respective pH-optimum, with 100% corresponding to 120.2 units/mg (ABTS) and 1.83 units/mg (guaiacol), respectively. In all figures, the mean value of triple measurements is given. *E* and *F,* mass spectrometric analysis of the formation of TauBr in the absence (*E*) and presence (*F*) of LspPOX (H_2O_2).

which showed the formation of two typical TauCl peaks with *m*/*z* values of 157.98 and 159.98, respectively (data not shown).

Besides two-electron oxidation reactions, LspPOX also catalyzed typical peroxidase reactions using artificial one-electron donors like guaiacol and ABTS. Whereas guaiacol is oxidized over a broad pH range (maximum around pH 4.5), reasonable ABTS oxidation rates were only observed in the acidic region (Fig. 7*D*).

Unfolding Pathway and Thermal Stability—Finally, we have analyzed whether the autocatalytic covalent bond formation between the prosthetic group and the protein has an impact on the conformational stability. Fig. 4*A* shows that both LspPOX and LspPOX (H_2O_2) exhibited exactly the same far-UV ECD spectrum suggesting identical overall secondary structure content with dominating α-helices (minima at 208 and 222 nm). By contrast, when focusing on the ellipticity of the heme Soret region, clear differences were seen (Fig. 4*B*). The minimum at 408 nm of LspPOX was shifted upon preincubation with H_2O_2 to 411 nm with concomitant peak sharpening and an increase in ellipticity suggesting formation of a more rigid (asymmetric) heme environment.

Next, we probed whether the covalent links between the heme group and the protein might have an impact on the conformational and thermal stability. DSC measurements of LspPOX and LspPOX (H_2O_2) were performed at different pH regimes (Fig. 8). Around neutral pH, LspPOX showed two endotherms (T_m values at 72.6 and 80.1 °C) clearly suggesting two independent unfolding events. At acidic pH values, both

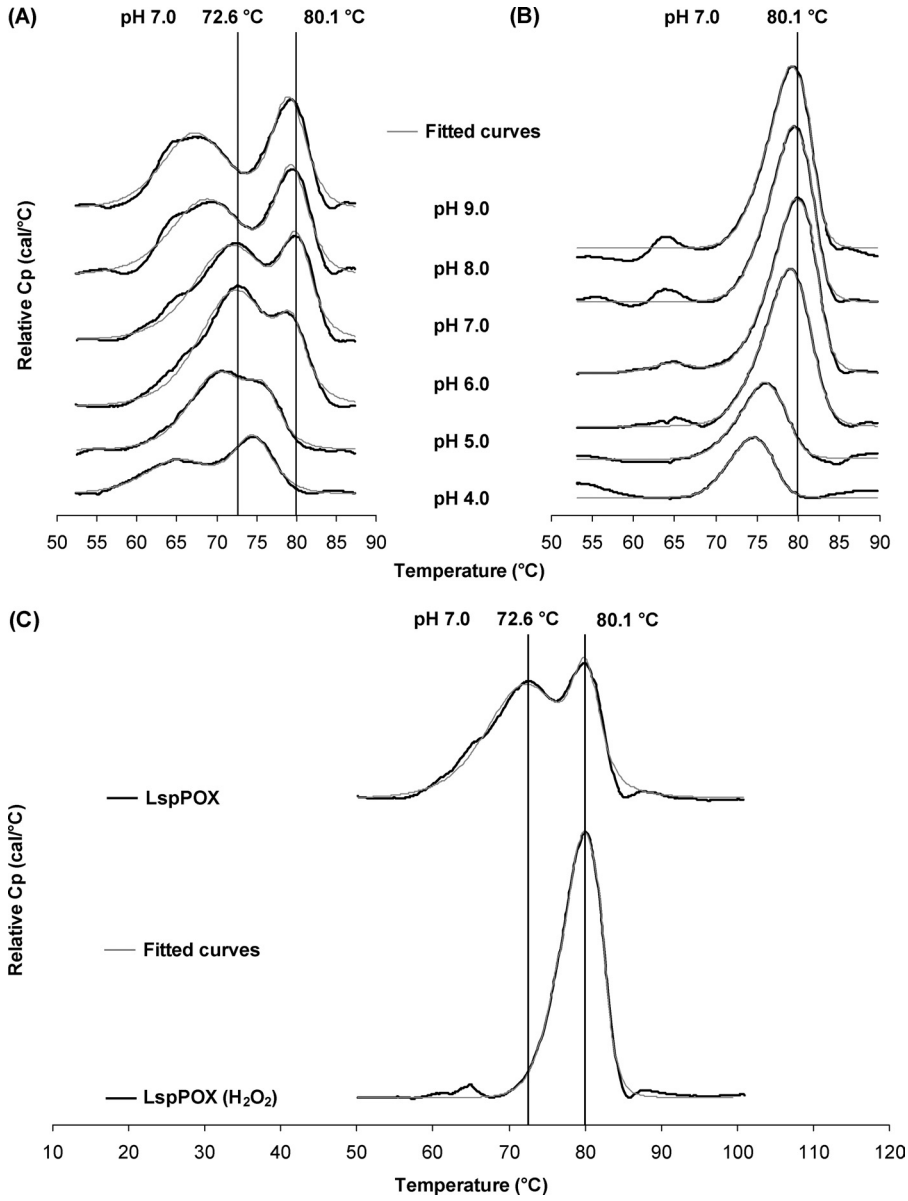

FIGURE 8. **Thermal stability of heme peroxidase from *Lyngbya* PCC 8106 monitored by differential scanning calorimetry.** Normalized DSC thermograms of LspPOX (*A*) and LspPOX (H_2O_2) (*B*) at different pH values after base-line subtraction. Fits of experimental data (*black line*) to a non-two-state model are shown in *gray*. Conditions are as follows: 5 μM enzyme in 10 mM carbonate buffer (pH 9.0–11.0) or 10 mM phosphate buffer (pH 5.0-pH 8.0) or 10 mM citrate phosphate buffer (pH 3.0-pH 5.0) and 0.5 M guanidinium hydrochloride to prevent aggregation during heating. Heating rate is 90 °C/h; temperature range is 20–100 °C; cell pressure is 30 p.s.i. (4.1 bar). *C,* comparison of thermograms of LspPOX and LspPOX (H_2O_2) at pH 7.0.

endotherms exhibited lower T_m values, and below pH 5.0 aggregation was observed, whereas at more basic pH values, only the maximum of the first endotherm shifted to lower T_m values (Fig. 8*A*).

LspPOX (H_2O_2) showed a completely different thermal unfolding pattern (Fig. 8*B*). Covalently linking the heme to the protein resulted in a more compact overall structure and led to only one endotherm that could be fitted to a simple two-state transition (T_m = 80.1 °C at pH 7.0). No differences were seen between pH 6 and 9 (except some aggregation events around 65 °C at pH 8 and 9), whereas the thermal stability at acidic pH values decreased and some protein precipitated during temperature increase. Fig. 8*C* highlights these significant differences in the thermal stability of native and H_2O_2-preincubated LspPOX at pH 7.0.

Following the loss of ellipticity mediated by temperature at 208 and 409 nm by ECD confirmed that covalently bound heme increased the thermal stability. Moreover, the observed loss of ellipticity at the Soret region suggested that unfolding of the active site could be attributed to the second unfolding event in LspPOX or occurred cooperatively with the overall unfolding in LspPOX (H_2O_2) (Fig. 9, *A* and *B*).

The high thermal stability of LspPOX is also reflected by the impact of temperature on the brominating as well as peroxidase activity (Fig. 9, *C* and *D*). The enzymes were slowly heated and kept at the respective temperature for 5 min. After cooling to room temperature, the enzyme activity was measured. The bacterial peroxidase showed almost no loss of activity after heat incubation up to 60 °C. Even after incubation at 70 °C, it still exhibited more that 50% brominating and peroxidase activity,

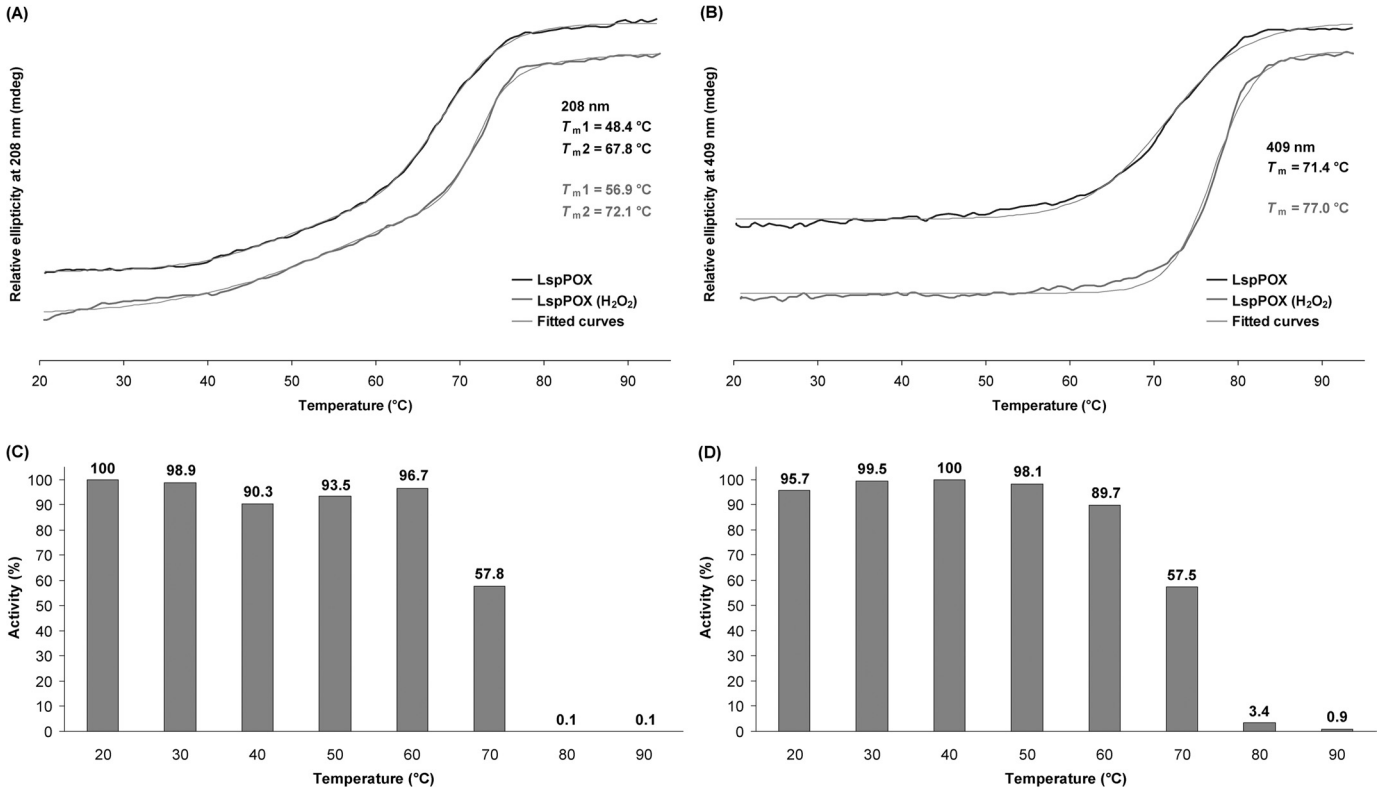

FIGURE 9. **Thermal stability of heme peroxidase from *Lyngbya* PCC 8106.** *A,* temperature-mediated unfolding monitored by electronic circular dichroism at 208 nm following melting of α-helical structures. *B,* temperature-mediated unfolding monitored by electronic circular dichroism at 409 nm following unfolding of the heme cavity. *C,* temperature-dependent halogenation activity upon following bromide oxidation by the MCD assay at pH 7.0. Conditions are as follows: 100 mM bromide, 100 μM H_2O_2, 5 nM LspPOX, 100 mM phosphate buffer, pH 7.0. *D,* temperature-dependent peroxidase activity following ABTS oxidation. Conditions are as follows: 1 mM ABTS, 100 μM H_2O_2, 25 nM LspPOX, 100 mM phosphate buffer, pH 7.0. For details of incubation see "Experimental Procedures." The average of three measurements is given.

which nicely reflected the observation that the (cooperative) unfolding process of LspPOX (H_2O_2) started at temperatures above 70 °C (Figs. 8 and 9*B*).

DISCUSSION

Analysis of the recently constituted peroxidase-cyclooxygenase superfamily suggested that the peroxidase domains found in five out of seven subfamilies show structural similarity with the vertebrate (including human) enzymes (subfamily 1) that constitute the cornerstone of the innate immune system. The observed early differentiation in the evolutionary history of this superfamily thus might give some insight into the evolution of unspecific defense reactions (2, 26). Before organisms developed an acquired immune system, their (anti-microbial) defense depended (among others) on enzymes like peroxidases that were recruited upon pathogen attack or invasion and efficiently produced halogenating and oxidizing antimicrobial products like hypohalous acids and hypothiocyanite (5, 23).

It has been demonstrated that one of the most important structural features of halogenating enzymes (*e.g.* LPO and EPO) is the modification of the 1- and 5-methyl groups on pyrrole rings A and C of the heme group allowing formation of ester linkages with the carboxyl groups of conserved glutamate and aspartate residues (4, 23). Myeloperoxidase is unique in having a third covalent bond, which connects the β-carbon of the vinyl group on pyrrole ring A with the sulfur atom of methionine 243 giving rise to an additional sulfonium ion linkage (24, 27, 28). Formation of these covalent heme-protein bonds has been proposed to occur autocatalytically (29–32) and has a deep impact on the biochemical and biophysical properties of these mammalian peroxidases (23, 24, 33).

This study has demonstrated that the heme group in the bacterial ancestor of these enzymes is also covalently bound to the protein, most probably via ester bond(s) between a conserved aspartate (Asp-100) and/or glutamate residue (Glu-229) very similar to lactoperoxidase (Fig. 2) (13). Participation of Glu-229 in heme binding could be shown by LC-MS. Whether Asp-100 contributes to heme binding remains unclear.

It was interesting to see that the recombinant protein produced by *E. coli* contained mainly unmodified heme *b*. This indicates that the peroxide concentration within the host organism was too low for triggering the autocatalytic post-translational modification. An external addition of a 15 times molar excess of H_2O_2 to the recombinant peroxidase was sufficient to convert the metalloprotein to compound I. This electron-deficient intermediate then most probably must have oxidatively attacked the nearby located carboxyl side chains of glutamate 229 (and possibly Asp-100) for ester bond formation. During this process, the symmetry of the heme group as well as its planarity were lowered, and its rigidity was increased. This was evident by the described changes of the UV-visible ECD as well as EPR spectra. Similar to LPO (25), the bacterial peroxidase showed two ferrous forms with the intermediate state being

stabilized after modification of the heme group by hydrogen peroxide and featuring slightly different redox properties compared with the stable ferrous conformer. Moreover, upon cross-linking the heme with the protein, the enzyme became more compact and exhibited a higher conformational and thermal stability. In its mature form, it unfolded coordinatively in a simple two-state transition at a T_m of 80 °C.

Further evidence of the presence of covalently bound heme in LspPOX (H_2O_2) was the high standard reduction potential of -145 ± 10 mV, which compares with lactoperoxidase (-176 mV) and eosinophil peroxidase (-126 mV) (17). This $E^{0\prime}$ value is higher than in heme *b* peroxidases from the peroxidase-catalase superfamily (34) but is significantly lower than in myeloperoxidase (+5 mV) (18). The latter enzyme is unique due to its electron-withdrawing sulfonium ion linkage and its strongly distorted and asymmetric heme group. Because the proximal ligand histidine and its H-bonding partner Asn (Fig. 2*C*) (27, 28, 35) as well as the distal catalytic residues His, Arg, and Gln (Fig. 2, *A* and *B*) (4, 27, 28) seem to be fully conserved, it is reasonable to assume that the heme architecture in LspPOX (H_2O_2) resembles that of LPO (13) or EPO (unknown structure).

As a consequence of its more positive reduction potential, the oxidation capacity of the bacterial peroxidase is high. The cyanobacterial enzyme was more efficient in bromide oxidation than bovine lactoperoxidase and is an efficient catalyst of hypobromous acid production in the neutral pH region (Fig. 7*B*). Whereas in the neutral region the chlorination activity was negligible, it slightly increased by decreasing pH values. At pH 4.5, the specific activity of TauCl formation was about 3.4 units/mg (32% of MPO activity).

Thus, similar to the vertebrate counterparts, the bacterial peroxidase follows the halogenation cycle that is initiated by peroxide-mediated oxidation of the ferric protein to compound I, *i.e.* oxoiron(IV) plus porphyryl (Por) cation radical: (Fe(IV) = O···Por^{+}) (Reaction 1).

$$[\mathrm{Fe(III)\cdot\cdot Por}] + \mathrm{H_2O_2} \rightarrow [\mathrm{Fe(IV){=}O\cdot\cdot Por^{+}}] + \mathrm{H_2O}$$

REACTION 1

Compound I is directly reduced by the halide, X^-, to the ferric resting state, *i.e.* (Fe(III)···Por), thereby releasing hypohalous acids (HOX) (Reaction 2).

$$[\mathrm{Fe(IV){=}O\cdot\cdot Por^{+}}] + \mathrm{X^-} + \mathrm{H^+} \rightarrow [\mathrm{Fe(III)\cdot\cdot Por}] + \mathrm{HOX} + \mathrm{H_2O}$$

REACTION 2

It has been demonstrated that the hierarchy of $E^{0\prime}$ [Fe(III)/Fe(II)], *i.e.* MPO > EPO > LPO, follows the same trend that was observed for $E^{0\prime}$ of the compound I/Fe(III) couple, *i.e.* MPO (1160 mV) > EPO (1100 mV) > LPO (1090 mV) (36, 37). This suggests that $E^{0\prime}$ of the compound I/Fe(III) couple of mature LspPOX should be around 1100 mV at pH 7.0, which is consistent with the observed bromination activity at pH 7.0 (23, 33).

Detailed investigation of structure-function relationships of mammalian peroxidases was so far often hampered by the fact that LPO and EPO could be produced recombinantly only in very small amounts or even failed in production, whereas with MPO the production in CHO and HEK293 cell lines was possible but time-consuming and often accompanied by low heme occupancy. Now with this monomeric enzyme of high homology to LPO, we will be able to perform more and comprehensive mutational analyses that will help to study mechanistic questions in more detail. Moreover, LspPOX (H_2O_2) is extremely stable. In its mature form, the monomeric protein is compact and does not lose its structural integrity up to 70 °C, thereby outcompeting many peroxidases used in industry today. Its stability is reflected by the fact that even after incubation of LspPOX (H_2O_2) at higher temperatures, the enzyme did not lose its peroxidase and halogenation activity (Fig. 9). The mature bacterial protein unfolds in a simple two-state transition. Its T_m value is similar to that of MPO (38) but significantly higher than that of LPO (39). But, in contrast to the vertebrate peroxidases, the *Lyngbya* protein can easily be produced in *E. coli*, is monomeric, and is unglycosylated. Moreover, due to the fact that it does not contain disulfide bridges, it keeps its structural integrity even under reducing conditions (data not shown) where LPO or MPO are destabilized (38, 39). Thus, in the future this ancestral enzyme could be a new attractive and robust biocatalyst for one- and two-electron oxidation reactions in the industry.

The question remains about the physiological role of enzymes in bacteria that produce hypohalous acids. As already mentioned, in proteins of subfamily 5, the catalytic (peroxidase) domain is often associated with hemolysin-type toxins that are secreted to attack susceptible cells. Together with the release of oxidizing reaction products like hypobromous acid, this armory could be used for the attack of other organisms (thus promoting pathogenicity) or for defense against other organisms, including bacteria that lack this type of peroxidase and live in the same environment. Thus, in analogy with bacteriocins, which are proteinaceous toxins produced by bacteria to inhibit the growth of similar or related strains, the denomination peroxicin was introduced (2). Similar considerations may also hold for the sixth clade, including the *Lyngbya* peroxidase. The enzyme studied in this work is an exception because it does not contain additional domains. The inspection of the genomic context surrounding the LspPOX gene did not reveal any operon or gene cluster in which LspPOX might be involved. In contrast, it is transcribed as a single, medium-sized gene. However, most representatives of the fifth and sixth clade subfamilies (2) are also multidomain proteins with one catalytic (peroxidase) domain of high homology to LspPOX and Dockerin type I repeats. Those domains might also contribute in anchoring the catalytic domain to distinct scaffolds at the surface of cells (2).

However, so far no member of the fifth and sixth subfamily has an experimentally verified physiological function. Based on the presented biochemical data, such a study will contribute to our understanding of the evolution of innate immunity. Especially, it will help us to understand the small balance between the role of oxidizing and halogenating reaction products in simple host defense or attack reactions or, as has been recently demonstrated for human peroxidasin 1, in biosynthesis (40). The latter mammalian enzyme is also a heme peroxidase (with

homology to LPO or LspPOX) with additional (protein binding) domains.

Acknowledgment—We are grateful to Prof. Klaus Stolze (University of Veterinary Medicine, Vienna) who provided the EPR spectrometer for low temperature measurements.

REFERENCES

1. Zámocký, M., Furtmüller, P. G., and Obinger, C. (2010) Evolution of structure and function of class I peroxidases. *Arch. Biochem. Biophys.* **500,** 45–57
2. Zamocky, M., Jakopitsch, C., Furtmüller, P. G., Dunand, C., and Obinger, C. (2008) The peroxidase-cyclooxygenase superfamily: Reconstructed evolution of critical enzymes of the innate immune system. *Proteins* **72,** 589–605
3. Zamocky, M., and Obinger, C. (2010) in *Biocatalysis Based on Heme Peroxidases* (Torres, E., and Ayala, M., eds) pp. 7–30, Springer-Verlag, Berlin
4. Furtmüller, P. G., Zederbauer, M., Jantschko, W., Helm, J., Bogner, M., Jakopitsch, C., and Obinger, C. (2006) Active site structure and catalytic mechanisms of human peroxidases. *Arch. Biochem. Biophys.* **445,** 199–213
5. Arnhold, J., Monzani, E., Furtmüller, P. G., Zederbauer, M., Casella, L., and Obinger, C. (2006) Kinetics and thermodynamics of halide and nitrite oxidation by mammalian heme peroxidases. *Eur. J. Inorg. Chem.* **19,** 3801–3811
6. Davies, M. J., Hawkins, C. L., Pattison, D. I., and Rees, M. D. (2008) Mammalian heme peroxidases: from molecular mechanisms to health implications. *Antioxid. Redox Signal.* **10,** 1199–1234
7. Soudi, M., Zamocky, M., Jakopitsch, C., Furtmüller, P. G., and Obinger, C. (2012) Molecular evolution, structure, and function of peroxidasins. *Chem. Biodivers.* **9,** 1776–1793
8. Söderhäll, K. (1999) Invertebrate immunity. *Dev. Comp. Immunol.* **23,** 263–266
9. Dick, G. J., Podell, S., Johnson, H. A., Rivera-Espinoza, Y., Bernier-Latmani, R., McCarthy, J. K., Torpey, J. W., Clement, B. G., Gaasterland, T., and Tebo, B. M. (2008) Genomic insights into Mn(II) oxidation by the marine alphaproteobacterium *Aurantimonas* sp. strain SI85–9A1. *Appl. Environ. Microbiol.* **74,** 2646–2658
10. Tamura, K., Peterson, D., Peterson, N., Stecher, G., Nei, M., and Kumar, S. (2011) MEGA5: molecular evolutionary genetics analysis using maximum likelihood, evolutionary distance, and maximum parsimony methods. *Mol. Biol. Evol.* **28,** 2731–2739
11. Whelan, S., and Goldman, N. (2001) A general empirical model of protein evolution derived from multiple protein families using a maximum-likelihood approach. *Mol. Biol. Evol.* **18,** 691–699
12. Passardi, F., Theiler, G., Zamocky, M., Cosio, C., Rouhier, N., Teixera, F., Margis-Pinheiro, M., Ioannidis, V., Penel, C., Falquet, L., and Dunand, C. (2007) PeroxiBase: the peroxidase database. *Phytochemistry* **68,** 1605–1611
13. Singh, A. K., Singh, N., Sharma, S., Shin, K., Takase, M., Kaur, P., Srinivasan, A., and Singh, T. P. (2009) Inhibition of lactoperoxidase by its own catalytic product: crystal structure of the hypothiocyanate-inhibited bovine lactoperoxidase at 2.3-Å resolution. *Biophys. J.* **96,** 646–654
14. Gouet, P., Robert, X., and Courcelle, E. (2003) ESPript/ENDscript: Extracting and rendering sequence and 3D information from atomic structures of proteins. *Nucleic Acids Res.* **31,** 3320–3323
15. Bradford, M. M. (1976) A rapid and sensitive method for the quantitation of microgram quantities of protein utilizing the principle of protein-dye binding. *Anal. Biochem.* **72,** 248–254
16. Battistuzzi, G., Borsari, M., Ranieri, A., and Sola, M. (2002) Redox thermodynamics of the Fe^{3+}/Fe^{2+} couple in horseradish peroxidase and its cyanide complex. *J. Am. Chem. Soc.* **124,** 26–27
17. Battistuzzi, G., Bellei, M., Vlasits, J., Banerjee, S., Furtmüller, P. G., Sola, M., and Obinger, C. (2010) Redox thermodynamics of lactoperoxidase and eosinophil peroxidase. *Arch. Biochem. Biophys.* **494,** 72–77
18. Battistuzzi, G., Bellei, M., Zederbauer, M., Furtmüller, P. G., Sola, M., and Obinger, C. (2006) Redox thermodynamics of the Fe(III)/Fe(II) couple of human myeloperoxidase in its high-spin and low-spin forms. *Biochemistry* **45,** 12750–12755
19. Kettle, A. J., and Winterbourn, C. C. (1988) The mechanism of myeloperoxidase-dependent chlorination of monochlorodimedon. *Biochim. Biophys. Acta* **957,** 185–191
20. Doerge, D. R., Divi, R. L., and Churchwell, M. I. (1997) Identification of the colored guaiacol oxidation product produced by peroxidases. *Anal. Biochem.* **250,** 10–17
21. Childs, R. E., and Bardsley, W. G. (1975) The steady-state kinetics of peroxidase with 2,2′-azino-di-(3-ethylbenzthiazoline-6-sulphonic acid) as chromogen. *Biochem. J.* **145,** 93–103
22. Furtmüller, P. G., Jantschko, W., Regelsberger, G., Jakopitsch, C., Arnhold, J., and Obinger, C. (2002) Reaction of lactoperoxidase compound I with halides and thiocyanate. *Biochemistry* **41,** 11895–11900
23. Zederbauer, M., Furtmüller, P. G., Brogioni, S., Jakopitsch, C., Smulevich, G., and Obinger, C. (2007) Heme to protein linkages in mammalian peroxidases: impact on spectroscopic, redox and catalytic properties. *Nat. Prod. Rep.* **24,** 571–584
24. Brogioni, S., Stampler, J., Furtmüller, P. G., Feis, A., Obinger, C., and Smulevich, G. (2008) The role of the sulfonium linkage in the stabilization of the ferrous form of myeloperoxidase: a comparison with lactoperoxidase. *Biochim. Biophys. Acta* **1784,** 843–849
25. Ohlsson, P. I., and Paul, K. G. (1983) The reduction potential of lactoperoxidase. *Acta Chem. Scand. B.* **37,** 917–921
26. Santamaría-Hernando, S., Krell, T., and Ramos-González, M.-I. (2012) Identification of a novel calcium binding motif based on the detection of sequence insertions in the animal peroxidase domain of bacterial proteins. *PLoS One* **7,** e40698
27. Fiedler, T. J., Davey, C. A., and Fenna, R. E. (2000) X-ray crystal structure and characterization of halide-binding sites of human myeloperoxidase at 1.8 Å resolution. *J. Biol. Chem.* **275,** 11964–11971
28. Carpena, X., Vidossich, P., Schroettner, K., Calisto, B. M., Banerjee, S., Stampler, J., Soudi, M., Furtmüller, P. G., Rovira, C., Fita, I., and Obinger, C. (2009) Essential role of proximal histidine-asparagine interaction in mammalian peroxidases. *J. Biol. Chem.* **284,** 25929–25937
29. DePillis, G. D., Ozaki Si., Kuo, J. M., Maltby, D. A., and Ortiz de Montellano, P. R. (1997) Autocatalytic processing of heme by lactoperoxidase produces the native protein-bound prosthetic group. *J. Biol. Chem.* **272,** 8857–8860
30. Fayadat, L., Niccoli-Sire, P., Lanet, J., and Franc, J. L. (1999) Role of heme in intracellular trafficking of thyroperoxidase and involvement of H_2O_2 generated at the apical surface of thyroid cells in autocatalytic covalent heme binding. *J. Biol. Chem.* **274,** 10533–10538
31. Ortiz de Montellano, P. R. (2008) Mechanism and role of covalent heme binding in the CYP4 family of P450 enzymes and the mammalian peroxidases. *Drug. Metab. Rev.* **40,** 405–426
32. Huang, L., and Ortiz de Montellano, P. R. (2006) Heme-protein covalent bonds in peroxidases and resistance to heme modification during halide oxidation. *Arch. Biochem. Biophys.* **446,** 77–83
33. Battistuzzi, G., Stampler, J., Bellei, J., Vlasits, J., Soudi, M., Furtmüller, P. G., and Obinger, C. (2011) Influence of the covalent heme-protein bonds on the redox thermodynamics of human myeloperoxidase. *Biochemistry* **50,** 7887–7994
34. Battistuzzi, G., Bellei, M., Bortolotti, C. A., and Sola, M. (2010) Redox properties of heme peroxidases. *Arch. Biochem. Biophys.* **500,** 21–36
35. Stampler, J., Bellei, M., Soudi, M., Gruber, C., Battistuzzi, G., Furtmüller, P. G., and Obinger, C. (2011) Manipulating the proximal triad His-Asn-Arg in human myeloperoxidase. *Arch. Biochem. Biophys.* **516,** 21–28
36. Arnhold, J., Furtmüller, P. G., Regelsberger, G., and Obinger, C. (2001) Redox properties of the couple compound I/native enzyme of myeloperoxidase and eosinophil peroxidase. *Eur. J. Biochem.* **268,** 5142–5148
37. Furtmüller, P. G., Arnhold, J., Jantschko, W., Zederbauer, M., Jakopitsch, C., and Obinger, C. (2005) Standard reduction potentials of all couples of the peroxidase cycle of lactoperoxidase. *J. Inorg. Biochem.* **99,** 1220–1229
38. Banerjee, S., Stampler, J., Furtmüller, P. G., and Obinger, C. (2011) Conformational and thermal stability of mature dimeric human myeloperoxidase and a recombinant monomeric form from CHO cells. *Biochim. Bio-*

phys. Acta **1814,** 375–387
39. Banerjee, S., Furtmüller, P. G., and Obinger, C. (2011) Bovine lactoperoxidase, a versatile one- and two-electron catalyst of high structural and thermal stability. *Biotechnol. J.* **6,** 231–243
40. Bhave, G., Cummings, C. F., Vanacore, R. M., Kumagai-Cresse, C., Ero-Tolliver, I. A., Rafi, M., Kang, J.-S., Pedchenko, V., Fessler, L. I., Fessler, J. H., and Hudson, B. G. (2012) Peroxidasin forms sulfilimine chemical bonds using hypohalous acids in tissue genesis. *Nat. Chem. Biol.* **8,** 784–790
41. Stoll, S., and Schweiger, A. (2006) EasySpin, a comprehensive software package for spectral simulation and analysis in EPR. *J. Magn. Reson.* **178,** 42–55